



Holocene mountain glacier history in the Sukkertoppen Iskappe area, southwest Greenland



Avriel D. Schweinsberg ^{a,*}, Jason P. Briner ^a, Gifford H. Miller ^b, Nathaniel A. Lifton ^{c,d}, Ole Bennike ^e, Brandon L. Graham ^a

^a Department of Geology, University at Buffalo, Buffalo, NY, 14260, USA

^b INSTAAR and Department of Geological Sciences, University of Colorado, Boulder, CO, 80309, USA

^c Department of Earth, Atmospheric, and Planetary Sciences, Purdue University, West Lafayette, IN, 47906, USA

^d Department of Physics and Astronomy, Purdue University, West Lafayette, IN, 47906, USA

^e Geological Survey of Denmark and Greenland, Øster Voldgade 10, DK-1350, Copenhagen k, Denmark

ARTICLE INFO

Article history:

Received 21 March 2018

Received in revised form

11 June 2018

Accepted 12 June 2018

Available online 17 August 2018

Keywords:

Greenland

Holocene

Glacier fluctuations

Lake sediment

Cosmogenic *in situ* ¹⁴C

Neoglaciation

ABSTRACT

Mountain glaciers and ice caps (GIC) independent of the Greenland Ice Sheet respond rapidly to climate variations and records of their past extent provide information on the natural envelope of climate variability. Here, we use a multi-proxy approach that combines proglacial lake sediment analysis, cosmogenic nuclide surface-exposure dating (*in situ* ¹⁰Be and ¹⁴C), and radiocarbon dating of recently ice-entombed moss to generate a centennial-scale record of Holocene GIC fluctuations in southwestern Greenland. Following local deglaciation ~10–9 ka, sediments from proglacial Crash Lake record a glacier advance at ~9 ka that is indistinguishable from nearby ice sheet moraines, implying a synchronous response of GIC and the Greenland Ice Sheet to a centennial-scale climate event. Following this local glacier advance, GIC experienced net recession until ~4.6 ka. Radiocarbon ages of *in situ* moss ($n=29$) and Crash Lake sediments reveal intervals of glacier expansion at ~1.8, 1.2 and 0.7 ka that are superimposed on an overall trend of net glacier expansion throughout the late Holocene. *In situ* ¹⁴C concentrations from bedrock adjacent to radiocarbon-dated moss samples further constrain the duration of ice cover through the Holocene in this region. We find that our glacier-size proxy records during the past ~4 ka are broadly consistent with relatively lower temperatures recorded in GISP2 and occur during, or following, intervals of volcanic perturbations. Thus, we speculate that volcanic activity, although less frequent and intense than in the early Holocene and during the Little Ice Age, may have led to centennial-scale variability imprinted on net glacier expansion due to decreasing summer insolation through the late Holocene.

© 2018 Elsevier Ltd. All rights reserved.

1. Introduction

Progressive cooling throughout the Holocene in the Northern Hemisphere, primarily driven by a gradual reduction in summer insolation, has been punctuated by multi-decadal to millennial-scale climate variability (e.g., Mayewski et al., 2004; Wanner et al., 2008, 2011; Marcott et al., 2013; Solomina et al., 2015; Kobashi et al., 2017). Numerous studies document short-lived Holocene climate perturbations in terrestrial and marine archives in the Arctic and North Atlantic regions (e.g., Kobashi et al., 2011;

Larsen et al., 2012; Miller et al., 2013a; b; Geirsdóttir et al., 2013; Axford et al., 2009; Balascio et al., 2015; Schweinsberg et al., 2017), yet the spatio-temporal patterns of these climate changes and the forcing mechanisms that drive this variability remain under debate. Recent summaries (Wanner et al., 2008, 2011) suggest that a complex interaction of factors likely influenced Holocene climate, including Atlantic Meridional Overturning Circulation (AMOC) variability (McManus et al., 2004), meltwater forcing (Clark et al., 2001), solar irradiance (Bond et al., 2001; Wiles et al., 2004), explosive volcanism (Miller et al., 2012; Geirsdóttir et al., 2013; Kobashi et al., 2017), and internal unforced dynamics (Trouet et al., 2009), with increasing evidence for abrupt (Mayewski et al., 2004) and periodic (Denton and Karén, 1973; Bond et al., 2001) climate changes. Additional high-resolution archives of climate fluctuations

* Corresponding author.

E-mail address: avrielsc@buffalo.edu (A.D. Schweinsberg).

with vast spatial coverage are necessary to discern the leading mechanisms driving sub-millennial Holocene climate variability (Mayewski et al., 2004).

Although contemporary observations are critical for understanding the current mechanisms driving glacier behavior, geological reconstructions of mountain glacier and ice cap (GIC) fluctuations that extend beyond the instrumental period place constraints on the magnitudes of glacier responses to climate forcings, and illustrate the spatio-temporal variability of past climate. GIC are ideal for paleoclimatic reconstructions because they respond rapidly to small changes in glacier mass balance, and their records often preserve small-scale climatic signals, which are useful indicators of regional and global climatic changes (Oerlemans, 2005; Bakke et al., 2005). GIC reconstructions from the North Atlantic region demonstrate that GIC record centennial-scale climate variability superimposed on the millennial-scale insolation-driven cooling trend (Larsen et al., 2012; Geirsdóttir et al., 2013; Balascio et al., 2015). The non-linear nature of these sub-millennial-scale changes reflects both complex interactions in response to declining insolation, and the presence of additional climate drivers or strong local to regional feedbacks operating on varying timescales (Larsen et al., 2012; Geirsdóttir et al., 2013). Past centennial-scale variations in GIC extent have been linked to changes in ocean circulation in West and East Greenland (Balascio et al., 2015; Levy et al., 2014; Schweinsberg et al., 2017) and Iceland (Larsen et al., 2012). However, changes in ocean circulation have been attributed to solar forcing (Bond et al., 2001; Moffa-Sánchez et al., 2014; Jiang et al., 2015) and some modeling studies have confirmed that AMOC can switch between distinct modes in response to a small external forcing, such as solar variability (Jongma et al., 2007). Alternatively, late Holocene GIC fluctuations in Iceland (Larsen et al., 2011; Geirsdóttir et al., 2013), Baffin Island (Anderson et al., 2008; Miller et al., 2012), and on Disko island, West Greenland (Jomelli et al., 2016), suggest that periods of cooler temperatures (and glacial advances) are influenced by explosive volcanism and associated sea-ice/ocean feedbacks. Recently, volcanic forcing has been postulated as a driver of Holocene temperature fluctuations reconstructed from Greenland ice cores (Kobashi et al., 2017). In general, many studies postulate that sub-millennial scale Holocene climate variability was likely driven by a combination of mechanisms, yet regional discrepancies illustrate the ongoing need for additional continuous sub-millennial scale glacier and paleoclimate archives.

Few Holocene glacier records with centennial-scale resolution exist because in locations such as Greenland, extensive glacier advances during the last few hundred years commonly destroyed the geomorphic evidence of former glacier activity earlier in the Holocene (Gibbons et al., 1984; Kelly and Lowell, 2009). The majority of information on past local glacier activity in Greenland is fragmentary and primarily concerned with the timing of maximum extent and rates of twentieth century retreat (e.g., Citterio et al., 2010; Bjørk et al., 2012; Rastner et al., 2012; Bolch et al., 2013). Thus, little is known about local glacier evolution throughout the Holocene (Kelly and Lowell, 2009). Only a few studies have provided continuous records of Holocene mountain glacier fluctuations in East Greenland (Lowell et al., 2013; Levy et al., 2014; Balascio et al., 2015) and West Greenland (Fig. 1; Larsen et al., 2017; Schweinsberg et al., 2017).

In this study, we reconstruct Holocene GIC fluctuations at the centennial-scale in southwestern Greenland to 1) investigate the synchrony of GIC response to Holocene climate variability, and 2) explore climate forcing mechanisms that may have driven local glacier change during the Holocene. To achieve these objectives, we reconstruct GIC change in the Sukkertoppen region of southwest Greenland using proglacial lake sediment analysis, radiocarbon

dating of formerly ice-entombed *in situ* moss, and cosmogenic nuclide exposure dating of erratics (*in situ* ^{10}Be) and bedrock (*in situ* ^{14}C). We compare our glacier reconstructions with previously published local glacier records in the North Atlantic region and nearby Greenland Ice Sheet (GrIS) margin chronologies. Combined, the reconstructions reported here provide a comprehensive view of GIC change throughout the Holocene in the Sukkertoppen region of southwest Greenland, and complement the instrumental records by providing a longer temporal context within which to interpret the magnitude and rate of recent GIC changes (Marcott et al., 2013).

2. Study area

Local glaciers in the study region include the Sukkertoppen Iskappe (~2000 km², average thickness of ~300 m) and associated valley glacier outlets, a second large ice cap, Qaarajuttoq (~2000 km²), and the nearby ice caps and mountain glaciers on uplands from Søndre Isortoq to Søndre Strømfjord (Figs. 1 and 2; Weidick et al., 1992; Kelly and Lowell, 2009). The region is located between the coastline of Davis Strait and the western GrIS margin located ~200 km to the east. Sukkertoppen Iskappe and Qaarajuttoq, as well as the other nearby GIC, rest atop large, relatively flat plateaus that are dissected by Søndre Strømfjord, Eivedsfjord, and Søndre Isortoq, resulting in mountainous alpine topography that rises to more than 1700 m asl. These areas of high terrain support weathered bedrock tors and blockfields (felsenmeier) above presently glaciated terrain (Kelly, 1985), which have been utilized to decipher the long-term glacial history of the area (Beel et al., 2016; Strunk et al., 2017). The research area is underlain by Precambrian gneisses and granitic rocks with numerous intrusions of basaltic and diabasic dikes (Loewe et al., 1962; Henriksen, 2008). Many glaciers flow into the large glacial troughs that dissect the region, which routed inland ice streams to the coast and onto the continental shelf during previous expansions of the GrIS (Roberts et al., 2009, 2010).

3. Previous work in the Sukkertoppen region

Previous work in the Sukkertoppen region has primarily focused on reconstructing fluctuations of the GrIS margin from the Last Glacial Maximum (LGM; 26–19 ka; Clark et al., 2009) to present (Funder et al., 2011) with few studies on local glacier change. In our field area, the LGM ice margin likely extended to the continental shelf edge ~100 km offshore from the present coastline (Funder et al., 2011; Vasskog et al., 2015; Winsor et al., 2015b), and GIC across the Sukkertoppen area coalesced with the GrIS (Weidick, 1968).

Chronological data suggest that the GrIS margin reached the present day outer coastline between ~15 and 10 ka in areas to the north and south of the study region (Bennike and Björck, 2002; Larsen et al., 2014; Kelley et al., 2015; Winsor et al., 2015a; b). Several discontinuous moraine systems are preserved between the coast and the present-day margin of the GrIS indicating that retreat of the western GrIS margin during the Holocene was punctuated by stillstands or readvances (Weidick, 1968; Ten Brink, 1975; Kelly, 1985; Lesnek and Briner, 2018). Recently, the ages of two GrIS moraine belts preserved in the Sukkertoppen area were identified using ^{10}Be -dating; the western and eastern moraines belts are dated to $\sim 9.8 \pm 0.7$ ka and 9.0 ± 0.3 ka, respectively (Lesnek and Briner, 2018). These results suggest that many of the southern and eastern outlets of Sukkertoppen Iskappe and Qaarajuttoq may have been confluent with the GrIS during the early Holocene (Weidick, 1968; Lesnek and Briner, 2018). As a result, differentiating the deposits associated with local glaciation prior to this time is complex in the study region (Weidick, 1968).

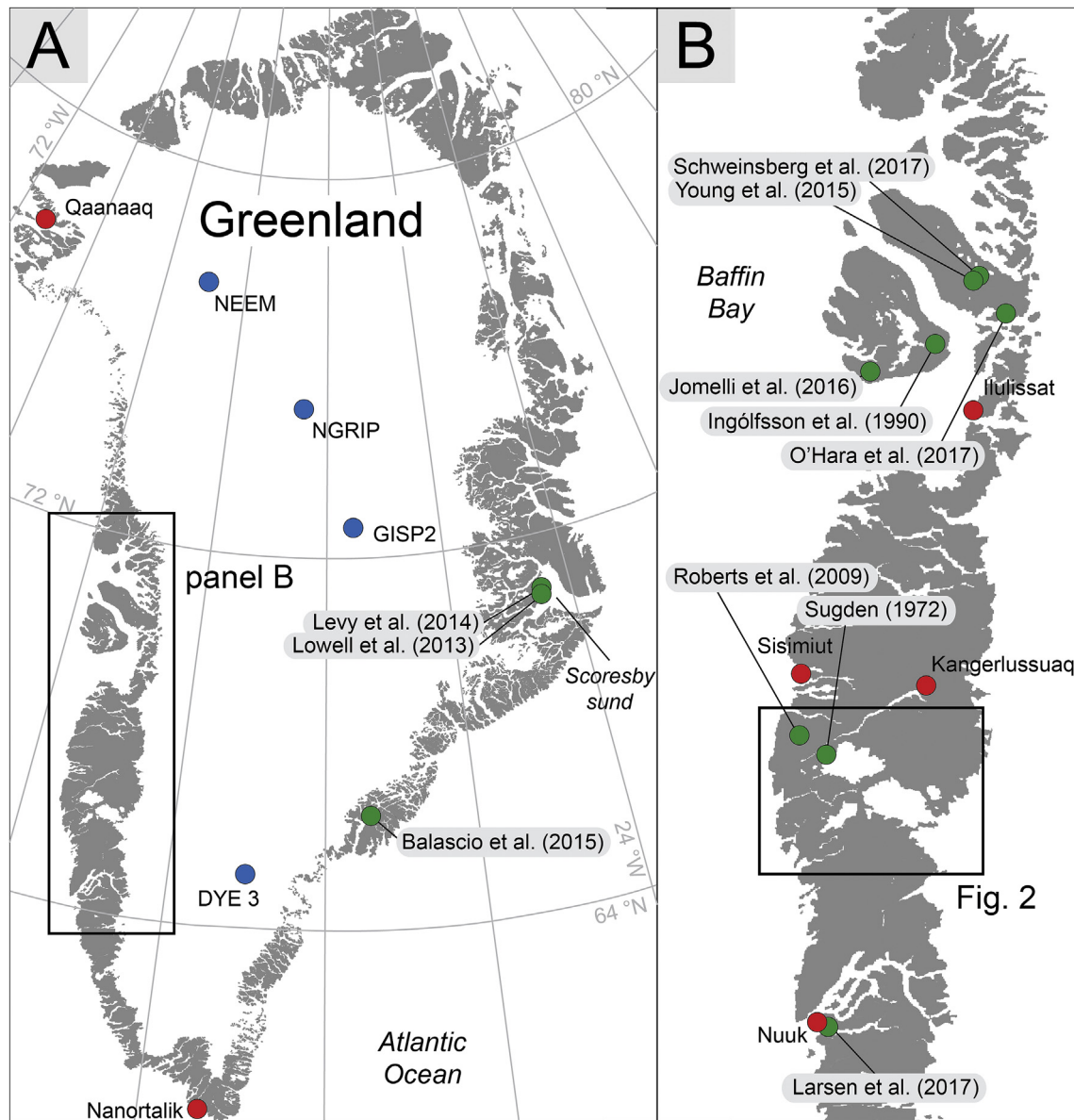


Fig. 1. Map of Greenland (panel A) showing studies discussed in the text (ice core drilling sites = blue circles, studies on Holocene local glacier fluctuations = green circles, communities = red circles). Panel B highlights previous studies on Holocene local glacier change in western Greenland. (For interpretation of the references to color in this figure legend, the reader is referred to the Web version of this article.)

Geological and glaciological expeditions in the Sukkertoppen region have been carried out since the early 1930s (e.g., Hayward, 1936; Mott, 1937; Sugden and Mott, 1940; Etienne, 1940; Cambridge West Greenland Glaciological Expedition, 1958, unpublished; Henry, 1959; Holland, 1961; Loewe et al., 1962; Bull, 1963), providing some of the earliest observations of local glaciers in the area. The majority of these reports focused on geological and glaciological mapping and reconnaissance, as well as describing the extents of local glaciers and the associated landforms of both mountain glaciers and the GrIS. As a result, the history of local glacier change in this region is primarily known from observations conducted throughout the 20th century (e.g., Weidick, 1968; Sugden, 1972; Kelly, 1985), recent satellite and remote-sensing-based studies (Rastner et al., 2012; Bolch et al., 2013; Machguth et al., 2016), and scant chronological data (Sugden, 1972).

The most detailed study of glacial geology and landforms in the Sukkertoppen area was conducted by Sugden (1972) and includes

observations of outlet glaciers emanating from the northern, eastern and southeastern edges of Sukkertoppen Iskappe. Sugden (1972) suggested that local glaciers were more extensive during the recent past due to the preservation of “fresh” moraines of ice cap outlet glaciers, which are undated and presumably deposited during the historical, or Little Ice Age (LIA) period (1200–1940 AD; Kelly and Lowell, 2009). Near Vimmelskaftet and Lyngbræ (ice cap outlets; Fig. 2), unvegetated moraines overlie or include marine sediments, and a single radiocarbon age (8430 ± 140 ^{14}C yr BP; 9400 ± 370 cal yr BP; K-1578) of shells in the Lyngbræ moraine indicates that this glacier was smaller at ~9.4 ka than during the LIA (Sugden, 1972). Similarly, one radiocarbon age (6510 ± 140 ^{14}C yr BP; 7400 ± 250 cal yr BP; K-1577) of mollusk shells in marine sediments at the head of Evighedsfjord also suggests restricted ice during the early to middle Holocene (Sugden, 1972). While Sugden (1972) proposed that the LIA moraines represent the maximum extent of GIC since deglaciation, Weidick (1968) observed pre-LIA

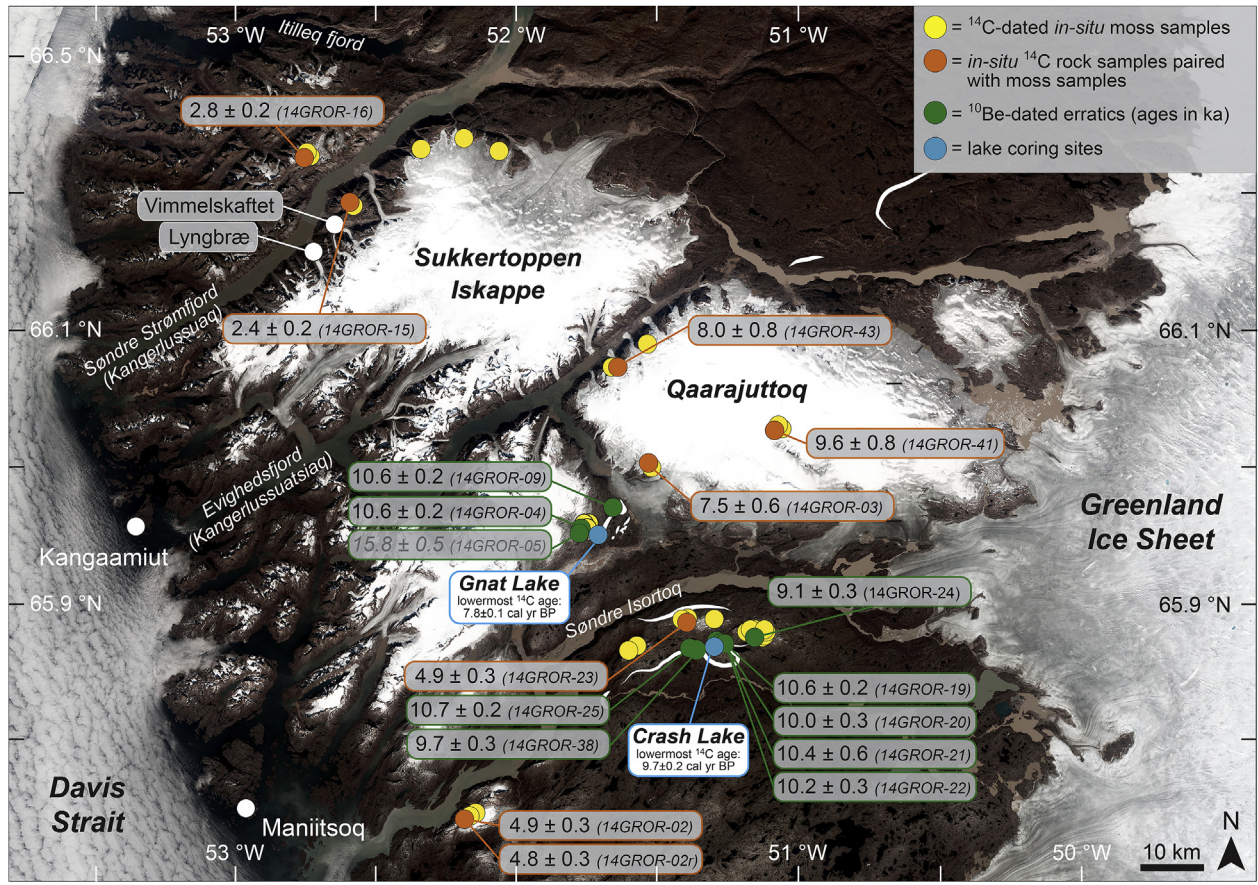


Fig. 2. Sukkertoppen study region with sample locations and *in situ* ^{14}C and ^{10}Be exposure ages used in this study. Yellow circles indicate radiocarbon-dated *in situ* tundra moss sample sites. Orange circles demarcate *in situ* ^{14}C apparent exposure ages (kyr) that are paired with moss samples. Green circles show locations of ^{10}Be -dated erratics (ka) while blue circles show lakes cored in this study. White lines reflect the general location of the early Holocene moraines in this region (Weidick, 1968; Ten Brink, 1975; Lesnek and Briner, 2018). White circles reflect communities. Base image is a Landsat8 natural color composite (RGB: 432) mosaic built with scenes acquired in July, August and September 2016. (For interpretation of the references to color in this figure legend, the reader is referred to the Web version of this article.)

moraines in at least five locations near the Sukkertoppen Iskappe, and suggested that the deposition of these moraines required glaciation limits ~200–400 m lower than at present. In addition, well-developed pre-LIA local glacier moraines have been reported on uplands ~100 km north of Søndre Strømfjord near Nordre Isortoq (Kelly, 1980), on Disko island (Ingólfsson et al., 1990; Jomelli et al., 2016), and the Nuussuaq peninsula (Fig. 1; Young et al., 2015; O'Hara et al., 2017). In general, most local glaciers reached a position near their LIA maximum between 1800 and 1900 AD in this region (Weidick, 1968; Kelly and Lowell, 2009).

4. Materials and methods

4.1. Sediment coring and analysis

During summer 2014, we cored two proglacial lakes ("Crash" and "Gnat" lakes; informal names; Figs. 2 and 3) to capture a continuous history of Holocene mountain glacier change in the Sukkertoppen region. We recovered sediment cores from each lake basin using a modified Universal Coring system (Nesje, 1992) deployed from an inflatable raft. A handheld GPS and a tape measure were used to determine the locations and water depths of the coring sites in each lake (Table 1), and bathymetric data were collected using an echo-sounder and Garmin GPSMAP 400 GPS device to determine locations most plausible for coring into deglacial material. To ensure that recently deposited sediments

remained intact, all cores were carefully recovered with undisturbed surface sediments overlain by clear lake water, and Zorbitrol was used to stabilize the sediment-water interface before transport (Tomkins et al., 2008). All sediment cores were packed in the field, shipped whole, and transported to the National Lacustrine Core Facility (LacCore) at the University of Minnesota, Minneapolis, MN, for core splitting and initial core processing and description. Prior to core splitting, sediment core density was measured at 0.5 cm intervals on a Geotek MSCL-S automated core logger. Core sections were then split longitudinally and core halves were photographed using a Geotek Geoscan linescan core imager, and magnetic susceptibility (MS) was measured continuously at 0.5 cm intervals on a Geotek MSCL-XYZ automated core logger. The working halves of each sediment core were subsequently transported to the University at Buffalo for sub-sampling while the archive halves were sent to the X-ray Fluorescence Laboratory at the University of Massachusetts-Amherst to acquire scanning X-ray fluorescence (XRF) data using an Itrax nondestructive core scanner to produce profiles of relative elemental compositions (Croudace et al., 2006; Rothwell et al., 2006).

In addition to MS, density, and geochemical analyses, sediments were analyzed for loss-on-ignition (LOI) to better characterize organic vs. minerogenic content. Trends in LOI values downcore are interpreted as changes in primary productivity loosely linked to summer temperature, as well as the dilution of organic matter by minerogenic sediment input (e.g., Balascio et al., 2015). Samples for

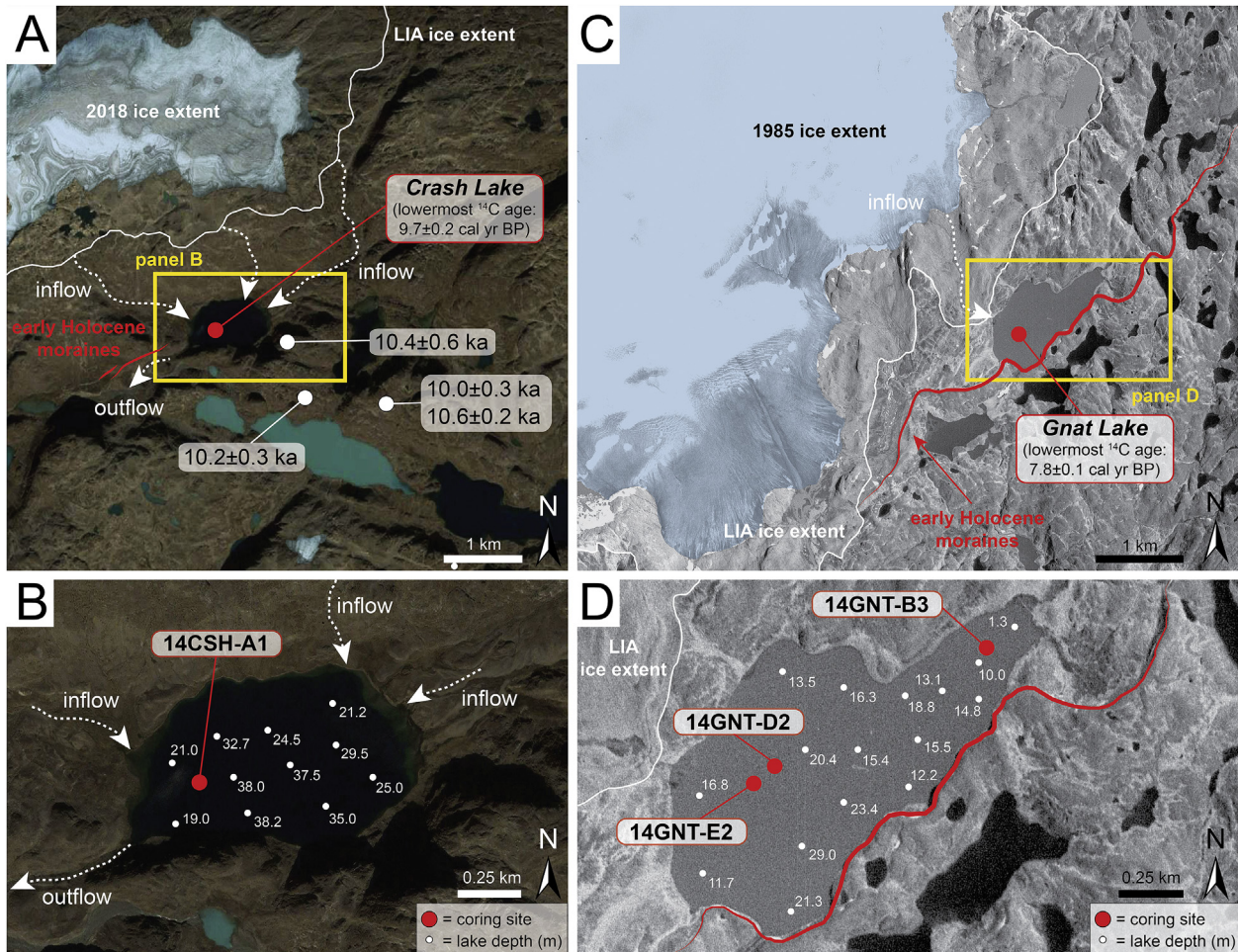


Fig. 3. Geologic setting and bathymetric data for investigated study lakes in the Sukkertoppen region. A) Crash Lake study site and meltwater routes. White circles demarcate ^{10}Be exposure ages previously published by Lesnek and Briner (2018). Base map is from Google Earth. B) Bathymetric data (white circles) and coring location (red circle) for Crash Lake. C) Gnat Lake study region and lake photograph. Base map is a 1985 aerial photograph. D) Coring sites (red circles) and bathymetric data (white circles) for Gnat Lake. Meltwater routes to Crash and Gnat lakes are shown by the white dashed lines in each panel. Red lines refer to mapped segments of early Holocene Greenland Ice Sheet moraines in this region (redrawn from Lesnek and Briner, 2018). (For interpretation of the references to color in this figure legend, the reader is referred to the Web version of this article.)

Table 1
Lake sediment core metadata.

Lake name	Core ID	Latitude ($^{\circ}\text{N}$)	Longitude ($^{\circ}\text{W}$)	Elevation (m asl)	Water depth (m)	Core length (cm)	Number of ^{14}C ages
Gnat Lake	14GNT-B3	65.83936	51.68837	489	14.0	58.5	2
Gnat Lake	14GNT-D2	65.83586	51.70262	489	24.6	93.0	1
Gnat Lake	14GNT-E2	65.83543	51.70440	489	25.0	86.5	1
Crash Lake	14CSH-A1	65.68131	51.29924	587	32.6	88.5	9

LOI analysis were taken from each sediment core at contiguous 0.5 cm intervals, and organic carbon was removed from the sediment during a 2.5-h burn at 550°C (Smith, 2003).

Age control of the lake sediments was established using Accelerator Mass Spectrometry (AMS) radiocarbon (^{14}C) dating (Table 2). Despite an extensive search, plant macrofossils were absent in the sediments and bulk sediment samples were selected for AMS ^{14}C analyses in all lake sediment cores. Bulk sediment samples were freeze-dried and homogenized prior to acid pretreatment (Abbot and Stafford, 1996) and measurement at the National Ocean Sciences AMS (NOSAMS) Facility (Woods Hole Oceanographic Institution). The lake catchments are dominated by felsic gneiss terrain similar to that of the Kangerlussuaq area for which Bennike et al. (2010) suggested that there was a small hardwater effect between

~ 100 and 200 ^{14}C years. Similarly, radiocarbon ages of bulk sediment are found to be ~ 230 years older than macrofossils from the same sediment interval in southwest Greenland sediment cores (Kaplan et al., 2002). All AMS ^{14}C results were calibrated and converted to calendar years before 1950 CE (cal yr BP) using CALIB v. 7.0 with the INTCAL13 calibration curve (Stuiver et al., 2005; Reimer et al., 2013), and are reported as the median of the 2σ range \pm half of the 2σ range (Table 2). The age-depth model for the Crash Lake sediment core (14CSH-A1) was constructed using a smooth spline interpolation between radiocarbon ages and a “basal” ^{10}Be age of $10.3 \pm 0.3 \text{ ka}$ ($n = 6$; Lesnek and Briner, 2018) and the classical age modeling (CLAM) code version 2.2 developed for the statistical program R (Blaauw, 2010). Because the water-sediment interface was captured and kept intact, the top

Table 2

Radiocarbon ages from lake sediment cores.

Core ID	Depth (cm)	Lab Number	Material Dated	Fraction Modern	$\delta^{13}\text{C}$ (‰ PDB)	Radiocarbon Age (^{14}C yr BP)	Calibrated Age (cal yr BP $\pm 2\sigma$)
<i>Crash Lake (informal name; proglacial lake)</i>							
14CSH-A1	8.5	OS-121813	sediment organic carbon	0.8288	-26.66	1510 \pm 15	1380 \pm 30
14CSH-A1	17.0	OS-121815	sediment organic carbon	0.7991	-26.79	1800 \pm 20	1720 \pm 90
14CSH-A1	31.0	OS-121816	sediment organic carbon	0.6756	-26.82	3150 \pm 25	3360 \pm 90
14CSH-A1	43.0	OS-121817	sediment organic carbon	0.5854	-26.92	4300 \pm 25	4890 \pm 60
14CSH-A1	48.5	OS-121818	sediment organic carbon	0.5498	-27.45	4810 \pm 25	5540 \pm 60
14CSH-A1	55.5	OS-121819	sediment organic carbon	0.4923	-26.92	5690 \pm 30	6480 \pm 70
14CSH-A1	62.0	OS-121814	sediment organic carbon	0.4417	-26.73	6560 \pm 35	7490 \pm 70
14CSH-A1	67.0	OS-132579	sediment organic carbon	0.3988	-26.31	7390 \pm 35	8200 \pm 130
14CSH-A1	74.0	OS-132746	sediment organic carbon	0.3441	-25.48	8570 \pm 95	9650 \pm 240
<i>Gnat Lake (informal name; proglacial lake)</i>							
14GNT-B3	11.5	OS-121809	sediment organic carbon	0.7275	-20.4	2560 \pm 20	2650 \pm 100
14GNT-B3	45.5	OS-121810	sediment organic carbon	0.4165	-23.32	7040 \pm 35	7870 \pm 80
14GNT-D2	29.0	OS-121811	sediment organic carbon	0.7951	-29.99	1840 \pm 20	1770 \pm 60
14GNT-E2	59.5	OS-121812	sediment organic carbon	0.7804	-29.17	1990 \pm 20	1940 \pm 50

sediment is set to the year of core recovery (2014 C.E.) in the Crash Lake age model. Radiocarbon ages in sediment cores 14GNT-B3, 14GNT-D2, and 14GNT-E2 were obtained to mark distinctive sedimentological transitions, and, therefore were not developed into an age-depth model due to the low number of radiocarbon ages per core. The lowermost radiocarbon ages from Crash and Gnat lakes are located 15.5 and 12.0 cm above the base of each core, respectively, and provide minimum-limiting age constraints of deglaciation in the region.

Principal component analysis (PCA) was used to characterize the patterns of variability in downcore parameters measured in Crash Lake sediments (Vasskog et al., 2012; Røthe et al., 2015; Schweinsberg et al., 2017). The parameters that exhibited an analytically robust signal (high signal-to-noise ratio) were included in the PCA, whereas the variables that had poor analytical measurements or low signal-to-noise ratios were excluded (Croudace et al., 2006). The higher resolution datasets (MS, density, XRF elemental data) were downsampled using AnalySeries 2.0.6 (Paillard et al., 1996) to obtain the same resolution as the parameter with the lowest resolution (LOI, every 0.5 cm) prior to PCA. For the PCA, the K/Ti ratio was used rather than Ti and K separately to remove fluctuations related to changing water content (Vasskog et al., 2012).

4.2. In situ moss chronology

4.2.1. Sample collection and field methodology

Following protocols described by previous studies (e.g., Miller et al., 2012, 2013a; b; 2017; Schweinsberg et al., 2017), sites for radiocarbon dating tundra moss were located along cold-based margins of GIC across the field area. Only demonstrably *in situ* plants, rooted and in growth position, were collected and then analyzed. Samples were collected from within one meter of the ice margin, where possible, to ensure that the plants were exposed during the year of collection (2014 C.E.), lowering the potential for anomalously young radiocarbon ages due to altered radiocarbon activity by plant regrowth (Miller et al., 2013b). Each sample was inspected for modern plant growth or re-

growth prior to collection, and samples were placed into an airtight collection bag. Geographic coordinates and sample elevations were obtained using a handheld GPS. The common *Polytrichum* moss genus was targeted for sampling due to its relatively brief life cycle (Miller et al., 2013a), however other moss genera were sampled and radiocarbon dated in the absence of *Polytrichum*, including: *Polytrichastrum*, *Racomitrium*, and *Polygonatum*. We avoided sampling woody plants (such as *Salix* sp.) and lichens because their survival potential after prolonged burial by ice is much greater than for moss, and their woody stems carry an average radiocarbon age older than their burial date (La Farge et al., 2013). Similarly, animal remains (i.e., bones, antlers, hides) were avoided in the field because the cause of death and precise ice margin position in relation to death is usually indeterminate (Miller et al., 2013b; Margreth et al., 2014).

4.2.2. Moss sample analysis

Macrofossils were isolated following standard procedures of wet sieving in deionized water to remove sediment and gentle sonication was performed when necessary. All plant material was examined using a binocular microscope and, if possible, a single stem of moss was selected for radiocarbon dating. We prefer to radiocarbon date a single moss stem because the radiocarbon age generally reflects a single year, and this technique minimizes the chance of dating a mixed-age sample (Miller et al., 2013b). If a single moss stem was not of sufficient mass (>2 mg), additional stems were selected until the desired mass was achieved. All samples were freeze-dried and weighed prior to AMS radiocarbon measurement. Moss samples were subsequently treated with an acid-base-acid wash, combusted, and converted to graphite at NOSAMS. The genus and species were identified for all radiocarbon-dated moss samples in this study (Table 3). Moss AMS ^{14}C ages were calibrated and converted to calendar years before 1950 CE (cal yr BP) using the downloadable version of CALIB 7.0 with the INTCAL13 calibration curve (Stuiver et al., 2005; Reimer et al., 2013). All calibrated ages are reported as the median of the 2σ range \pm half of the 2σ range uncertainty (Table 3).

Table 3

Tabulation of 34 radiocarbon dates on rooted mosses recently emerged from beneath glacier ice in the Sukkertoppen region and their metadata.

Sample ID	Lat. ($^{\circ}$ N)	Long. ($^{\circ}$ W)	Elev. (m asl)	Bedrock pair (if available)	Material dated	Distance from ice edge (cm)	Lab ID	Fraction modern	$\delta^{13}\text{C}$	^{14}C age	Calibrated age (cal yr BP $\pm 2\sigma$)	Calibrated age ranges
14GROV-04	65.41	52.15	983	—	<i>Polytrichum hyperboreum</i>	10	OS-113293	0.8564	-23.61	1240 \pm 20	1170 \pm 90	1082–1160, 1172–1194, 1196–1263
14GROV-05	65.66	51.56	887	—	<i>Polytrichum hyperboreum</i>	0	OS-113294	0.8547	-22.80	1260 \pm 20	1220 \pm 40	1176–1271
14GROV-07	65.66	51.55	893	—	<i>Polytrichum hyperboreum</i>	30	OS-114824	0.9319	—	565 \pm 15	580 \pm 50	535–560, 599–631
14GROV-08B	65.66	51.55	882	—	<i>Polytrichum hyperboreum</i>	0	OS-113343	0.9313	-25.28	570 \pm 15	590 \pm 50	537–561, 597–633
14GROV-09	65.70	51.38	975	—	<i>Polytrichastrum alpinum</i>	0	OS-113344	0.8596	-25.16	1210 \pm 15	1120 \pm 50	1068–1181
14GROV-10	65.670	51.39	990	14GROR-02	<i>Polytrichum piliferum</i>	80	OS-114825	0.8704	—	1110 \pm 20	1010 \pm 40	967–1058
14GROV-13	65.93	51.50	1160	14GROR-03	<i>Polytrichum hyperboreum</i>	200	OS-113345	0.7889	-21.26	1900 \pm 15	1850 \pm 30	1820–1881
14GROV-14A	65.84	51.73	668	—	<i>Polytrichum piliferum</i>	0	OS-114826	1.1071	—	>modern	modern	
14GROV-14B	65.84	51.73	668	—	<i>Polytrichum piliferum</i>	0	OS-114829	1.1807	—	>modern	modern	
14GROV-14C	65.84	51.73	668	—	<i>Polytrichum piliferum</i>	0	OS-114830	1.0742	—	>modern	modern	
14GROV-15	66.29	52.61	1399	14GROR-15	<i>Polytrichum piliferum</i>	40	OS-113346	0.6603	-24.08	3330 \pm 25	3560 \pm 80	3480–3538, 3544–3633
14GROV-17	66.37	52.76	1558	—	<i>Polytrichum hyperboreum</i>	0	OS-114908	0.6259	—	3760 \pm 20	4120 \pm 110	4008–4032, 4081–4160, 4171–4177, 4200–4227
14GROV-18	66.37	52.76	1557	—	<i>Polytrichum hyperboreum</i> , <i>Racomitrium lanuginosum</i>	0	OS-113347	0.6235	-25.90	3790 \pm 20	4170 \pm 80	4093–4126, 4142–4237
14GROV-19	66.37	52.76	1555	14GROR-16	<i>Racomitrium lanuginosum</i>	800	OS-114909	0.6167	—	3880 \pm 20	4330 \pm 80	4246–4408
14GROV-20	66.33	52.42	1597	—	<i>Polytrichum hyperboreum</i> , <i>Racomitrium lanuginosum</i>	0	OS-113381	0.7965	-26.03	1830 \pm 20	1770 \pm 60	1714–1820
14GROV-22	66.33	52.42	1595	—	<i>Polytrichum hyperboreum</i>	25	OS-113382	0.7904	-24.17	1890 \pm 20	1810 \pm 70	1741–1756, 1780–1800, 1805–1887
14GROV-23	66.38	52.35	1475	—	<i>Polytrichum piliferum</i>	0	OS-113383	0.7914	-25.79	1880 \pm 25	1810 \pm 70	1736–1879
14GROV-25	66.39	52.22	1402	—	<i>Polytrichum piliferum</i>	0	OS-113384	0.8665	-25.59	1150 \pm 25	1080 \pm 100	980–1098, 1101–1149, 1158–1173
14GROV-27	66.39	52.12	1322	—	<i>Polygonatum urnigerum</i>	0	OS-113385	0.9736	-22.10	215 \pm 20	150 \pm 150	1–12, 149–187, 210–210, 270–303
14GROV-28	66.39	52.12	1322	—	<i>Polygonatum urnigerum</i>	0	OS-114910	0.9789	—	170 \pm 20	140 \pm 140	1–31, 138–157, 165–222, 258–285
14GROV-31	65.70	51.28	901	—	<i>Polytrichum piliferum</i> , <i>Racomitrium lanuginosum</i>	0	OS-113386	0.8637	-26.19	1180 \pm 20	1100 \pm 90	1014–1016, 1057–1177
14GROV-33	65.69	51.18	982	—	<i>Polytrichum hyperboreum</i>	0	OS-113387	0.8077	-23.63	1710 \pm 30	1630 \pm 80	1554–1640, 1641–1698
14GROV-34	65.70	51.15	1013	—	<i>Polytrichum piliferum</i>	0	OS-114911	0.8583	—	1230 \pm 25	1170 \pm 100	1070–1189, 1201–1260
14GROV-36	65.69	51.15	1022	—	<i>Polytrichum hyperboreum</i> , <i>Racomitrium lanuginosum</i>	5	OS-113388	0.8079	-26.08	1710 \pm 25	1630 \pm 80	1555–1637, 1646–1697
14GROV-37	65.69	51.15	1022	14GROR-23	<i>Polytrichum piliferum</i>	1000	OS-114912	0.8234	—	1560 \pm 20	1460 \pm 60	1403–1524
14GROV-38	65.69	51.12	968	—	<i>Polytrichastrum alpinum</i>	0	OS-114913	0.9615	—	315 \pm 20	380 \pm 70	306–334, 349–439, 441–456
14GROV-39	65.69	51.12	968	—	<i>Poaceae indet. (grass)</i>	0	OS-114914	0.9727	—	225 \pm 30	160 \pm 160	1–15, 145–214, 267–309
14GROV-40	65.69	51.12	928	—	<i>Polytrichum hyperboreum</i> , <i>Pohlia cruda</i>	0	OS-113540	0.8485	-25.69	1320 \pm 15	1240 \pm 50	1187–1203, 1241–1249, 1255–1293
14GROV-43	65.98	51.07	1611	14GROR-41	<i>Racomitrium lanuginosum</i>	0	OS-113541	0.9185	-24.21	685 \pm 15	620 \pm 50	569–582, 650–674
14GROV-44	66.11	51.52	1398	—	<i>Polytrichum hyperboreum</i>	0	OS-113544	0.7933	-24.91	1860 \pm 15	1800 \pm 70	1730–1835, 1840–1864
14GROV-47A	66.06	51.66	1352	—	<i>Polytrichum piliferum</i>	0	OS-114915	0.7960	—	1830 \pm 25	1780 \pm 80	1704–1825, 1852–1858
14GROV-47B	66.06	51.66	1352	—	<i>Polytrichum piliferum</i>	0	OS-114916	0.7942	—	1850 \pm 30	1790 \pm 80	1715–1865
14GROV-47C	66.06	51.66	1352	—	<i>Polytrichum piliferum</i>	0	OS-114917	0.7917	—	1880 \pm 25	1810 \pm 70	1736–1879
14GROV-47D	66.06	51.66	1352	—	<i>Polytrichum piliferum</i>	0	OS-113599	0.7957	-24.49	1840 \pm 20	1770 \pm 60	1713–1825

4.3. Cosmogenic isotope analysis

4.3.1. ^{10}Be dating

Sampling of boulders for cosmogenic ^{10}Be surface-exposure dating (hereafter ^{10}Be dating) follows protocols described for previous investigations (Fig. 4; e.g., Kelley et al., 2013; Young et al., 2015; Cronauer et al., 2016; Lesnek and Briner, 2018). Nine ^{10}Be ages on perched boulders previously published by Lesnek and Briner (2018) provide constraints on deglaciation in the study area; see Lesnek and Briner (2018) for additional sample details and methods. Here, we report an age for one additional quartz-rich boulder (14GROR-24) to provide constraints on local deglaciation. All ^{10}Be ages reported here are calculated using the CRONUS-Earth online exposure age calculator (Tables 4 and 5; Balco, 2017; version 3; <http://hess.ess.washington.edu/>) using the locally-constrained Baffin Bay/Arctic production rate (Young et al., 2013a) with the LSDn scaling scheme (Lifton et al., 2014, 2015, Table 5).

4.3.2. In situ ^{14}C

We complement radiocarbon dating of *in situ* moss by measuring cosmogenic *in situ* ^{14}C inventories in recently exposed bedrock surfaces adjacent to the moss samples (Figs. 2 and 5; Anderson et al., 2008; Miller et al., 2006). We use *in situ* ^{14}C concentrations to provide an independent evaluation of the moss radiocarbon ages, and to constrain the total cumulative burial duration in the Holocene. Building on work completed by Anderson et al. (2008), we model plausible exposure-burial scenarios for each moss-bedrock pair during the Holocene.

In situ ^{14}C samples were collected in the field using methods similar to those described in section 3.5.3.1. for ^{10}Be dating and are reported in Table 6. All physical and chemical processing of *in situ* ^{14}C samples was conducted in the Purdue Rare Isotope Measurement Laboratory (PRIME Lab) at Purdue University, West Lafayette, IN. *In situ* ^{14}C was extracted from purified quartz separates from each bedrock site (Table 6) using newly refined methods at PRIME Lab (Lifton et al., 2015). The automated extraction process involves combusting ~5–10 g of quartz at 600 °C for one hour to remove

atmospheric contaminants, followed by dissolution in a degassed LiBO₂ flux at 1100 °C for three hours. Both steps take place in an atmosphere of ca. 50 torr of Research Purity O₂. Any carbon species released during the high-temperature step are oxidized to CO₂, which is then purified, measured quantitatively, and converted to graphite for ^{14}C measurement by AMS at PRIME Lab (Lifton et al., 2015). *In situ* ^{14}C concentrations are calculated from measured AMS isotope ratios following Hippe and Lifton (2014). 14GROR-02r is a replicate sample of 14GROR-02 and was a separate extraction on a different quartz aliquot.

Exposure-burial histories were modeled in Matlab r2017b. Each sample is modeled using the default CRONUS *in-situ* ^{14}C production rate (Borchers et al., 2016; Phillips et al., 2016; Balco, 2017) and the LSDn scaling framework (Lifton et al., 2014, 2015). Each scenario is modeled with different ice thicknesses to account for the effects of muogenic production beneath thin ice cover (e.g., Miller et al., 2006; Hippe, 2017), and to assess the influence of ice thickness on the duration of burial at each site through the Holocene.

5. Results and interpretation

5.1. Lacustrine sediment records

Three sediment cores were recovered from Gnat Lake (Fig. 6, Tables 1 and 2). Sediment cores 14GNT-B3, 14GNT-D2, and 14GNT-E2 are 58.5, 93.0, and 86.5 cm-long, respectively, and display similar downcore stratigraphy but with varying unit thicknesses (Fig. 6). Cores 14GNT-B3 and 14GNT-D2 are composed of a basal unit of gray mineral-rich sediment, middle units of laminated organic-rich sediment, and a top unit of light gray mineral-rich sediments that grade to yellow (Fig. 6). Basal mineral-rich sediments were not recovered in sediment core 14GNT-E2 because the basal unit is composed of light brown laminated organic-rich sediments that are overlain by a light gray mineral-rich unit that grades to yellow. Despite the variable stratigraphy between Gnat Lake sediment cores, the transition from organic-rich to mineral-rich sediments is preserved in the upper section of each sediment



Fig. 4. Photographs of selected boulders sampled for ^{10}Be dating in this study and Lesnek and Briner (2018). 14GROR-04, 14GROR-21 and 14GROR-22: Perched boulders on bedrock outboard of the Fjord Stade moraines in the Sukkertoppen region (Lesnek and Briner, 2018). 14GROR-24: Perched boulder on bedrock (this study).

Table 4

Sample collection and laboratory information for the ^{10}Be samples used to constrain deglaciation in the Sukkertoppen region. All ^{10}Be ages are previously published by [Lesnek and Briner \(2018\)](#) except for 14GROR-24 (this study).

Sample ID	Latitude ($^{\circ}\text{N}$)	Longitude ($^{\circ}\text{W}$)	Elevation (m asl)	Thickness (cm)	Shielding correction	Quartz (g)	Carrier added (g) ^a	$[^{10}\text{Be}]$ (atoms g $^{-1}$)	\pm (atoms g $^{-1}$)
14GROR-04	65.83537	51.72836	494.7	2.0	0.9987	26.1162	0.6053	7.32E+04	1.55E+03
14GROR-05	65.83521	51.72817	537.7	2.0	0.9981	22.3277	0.6077	1.13E+05	3.61E+03
14GROR-09	65.86336	51.61453	639.9	1.5	0.9993	25.0896	0.6078	1.17E+05	2.13E+03
14GROR-19	65.67472	51.25421	772.0	2.0	0.9980	18.0407	0.6078	9.49E+04	1.85E+03
14GROR-20	65.67473	51.25575	784.7	2.0	0.9990	20.9872	0.6095	9.01E+04	2.30E+03
14GROR-21	65.67440	51.27269	689.0	2.0	0.9942	18.9835	0.6081	8.58E+04	4.79E+03
14GROR-22	65.67799	51.28418	756.3	2.0	0.9987	18.1967	0.6075	9.01E+04	2.55E+03
14GROR-24	65.68883	51.13035	1021.3	2.0	0.9994	17.2862	0.6088	1.02E+05	3.20E+03
14GROR-25	65.65844	51.36256	524.5	2.0	0.9991	29.9937	0.6078	7.57E+04	1.50E+03
14GROR-38	65.66175	51.35546	628.8	3.0	0.9964	18.3615	0.6094	7.73E+04	2.22E+03

^a Samples were prepared using a carrier with a ^{9}Be concentration of 372.5 ± 3.5 ppm (GFZ Q2 14/10/2010).

Table 5

Comparison of ^{10}Be exposure ages (yrs) calculated with alternative production rates and scaling schemes. All ^{10}Be ages were calculated using version 3 of the CRONUS-Earth online exposure age calculator ([Balco, 2017](#)).

Sample ID	^{10}Be ages calculated using Arctic/Baffin Bay PR ^{a,c}			^{10}Be ages calculated using CRONUS default PR ^{b,c}		
	St	Lm	LSDn (Table 3)	St	Lm	LSDn
14GROR-04	10400 ± 200	10400 ± 200	10600 ± 200	10300 ± 200	10000 ± 200	9700 ± 200
14GROR-05	15500 ± 500	15500 ± 500	15800 ± 500	15300 ± 500	14800 ± 500	14400 ± 500
14GROR-09	10400 ± 200	10400 ± 200	10600 ± 200	10300 ± 200	10000 ± 200	9700 ± 200
14GROR-19	10500 ± 200	10500 ± 200	10600 ± 200	10300 ± 200	10000 ± 200	9700 ± 200
14GROR-20	9800 ± 300	9800 ± 300	10000 ± 300	9700 ± 300	9400 ± 200	9100 ± 200
14GROR-21	10200 ± 600	10200 ± 600	10400 ± 600	10100 ± 600	9800 ± 600	9500 ± 500
14GROR-22	10100 ± 300	10100 ± 300	10200 ± 300	9900 ± 300	9700 ± 300	9300 ± 300
14GROR-24	9000 ± 300	9000 ± 300	9100 ± 300	8900 ± 300	8600 ± 300	8300 ± 300
14GROR-25	10500 ± 200	10500 ± 200	10700 ± 200	10300 ± 200	10000 ± 200	9700 ± 200
14GROR-38	9800 ± 300	9800 ± 3000	10000 ± 300	9700 ± 300	9400 ± 300	9100 ± 300

^a ^{10}Be ages calculated using the Arctic/Baffin Bay production rate ([Young et al., 2013a](#)).

^b ^{10}Be ages calculated using the default production rate ([Borchers et al., 2016; Balco, 2017](#)).

^c ^{10}Be exposure ages are calculated using a sample density of 2.65 g cm^{-3} and an effective attenuation length of 160 g cm^{-2} . We assume zero erosion over these timescales. All ^{10}Be concentrations are reported relative to 07KNSTD3110 with a reported ratio of 2.85×10^{-12} using a ^{10}Be half-life of 1.36×10^6 years ([Nishiizumi et al., 2007](#)). The reported ratios have already been blank-corrected (the batch-specific process blank ratios ranged from 4.9×10^{-15} to 1.0×10^{-15}). Reported uncertainties are internal AMS uncertainties. We note that these exposure ages are not corrected for time-dependent altitudinal changes associated with glacio-isostatic adjustment.

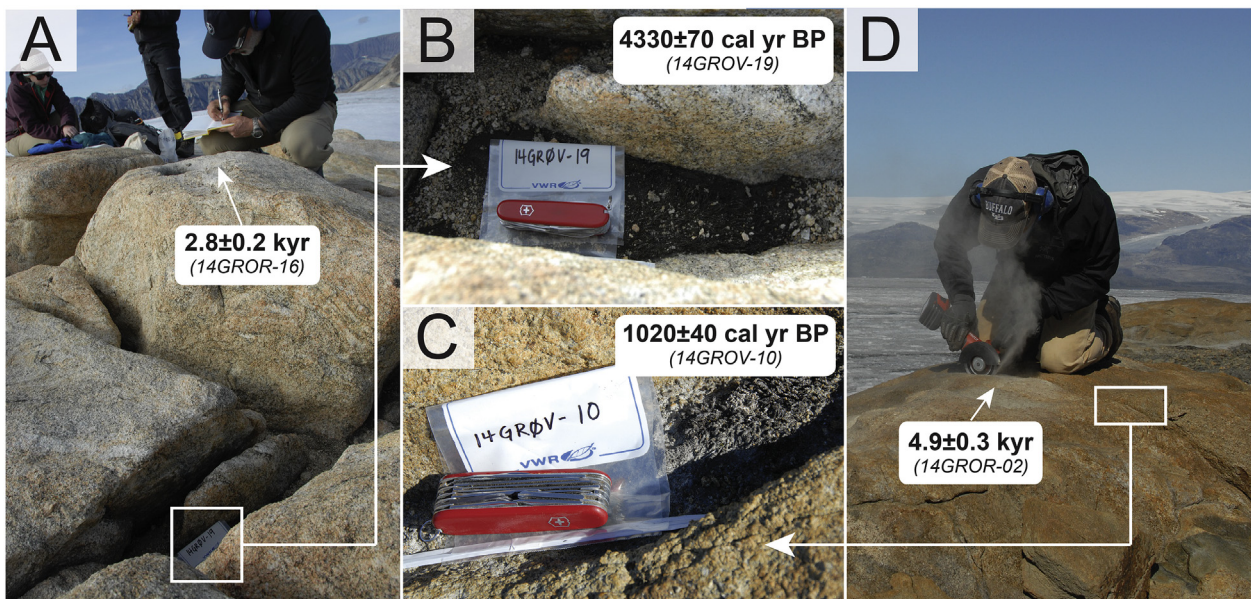


Fig. 5. Representative photographs showing two moss-bedrock pairs in the Sukkertoppen study area. (A) Recently exposed bedrock sample for *in situ* ^{14}C measurement (14GROR-16), and (B) paired moss sample (14GROV-19). (C) Rooted moss sample (14GROV-10), and (D) paired *in situ* ^{14}C bedrock sample (14GROR-02). Black text reflects the *in situ* ^{14}C apparent exposure age (bedrock) or conventional calibrated radiocarbon age (moss).

Table 6Sample collection, laboratory information and apparent exposure ages for *in situ*¹⁴C samples in the Sukkertoppen region.

Sample ID	Paired moss sample	Latitude	Longitude	Elev.	Thickness	Quartz	[¹⁴ C]	±	Exposure age (LSDn) ^a	±	Exposure age (Lm)	±
		(°N)	(°W)	(m asl)	(cm)	(g)	(atoms g ⁻¹)	(atoms g ⁻¹)	(yr/BP)	(yr/BP)	(yr/BP)	(yr/BP)
14GROR-02	14GROV-10	65.69620	-51.38621	988	2.5	10.1	152,501	4880	4900	300	5200	400
14GROR-02	14GROV-10	65.69620	-51.38621	988	2.5	10.0	149,904	4986	4800	300	5100	400
14GROR-03	14GROV-13	65.93228	-51.50253	1162	2.5	5.0	235,523	8040	7500	600	8200	800
14GROR-15	14GROV-15	66.29484	-52.60547	1400	3.0	10.0	122,649	5960	2400	200	2600	200
14GROR-16	14GROV-19	65.97910	-51.07040	1613	2.0	10.0	159,429	4999	2800	200	3100	200
14GROR-23	14GROV-37	65.69131	-51.15436	1022	2.0	10.0	157,986	4469	4900	300	5300	400
14GROR-41	14GROV-43	66.37012	-52.76334	1558	4.0	10.0	385,769	6880	9600	800	11000	1200
14GROR-43	N/A	66.06223	-51.65926	1351	1.5	5.1	289,189	12,367	8000	800	8900	1000

^a Apparent *in situ*¹⁴C exposure ages are calculated using a time-integrated production rate and LSDn scaling (13.0 ± 0.5 atoms g⁻¹ yr⁻¹; Lifton et al., 2015; Borchers et al., 2016; Phillips et al., 2016; Balco, 2017), a sample density of 2.65 g cm⁻³, a standard of OKNSTD, and topographic shielding correction of 1 (shielding was negligible at all sample sites). We assume zero erosion over these timescales. The following blank corrections have been subtracted from the total number of ¹⁴C atoms measured for given samples: 14GROR-02, -15, -16, -41 = $(2.98 \pm 0.37) \times 10^5$ ¹⁴C atoms; 14GROR-02, -03, -23, -43 = $(1.54 \pm 0.31) \times 10^5$ ¹⁴C atoms. AMS data reduction follows Hippe and Lifton (2014). Similar to the *in situ*¹⁰Be ages, *in situ*¹⁴C exposure ages are not corrected for time-dependent altitudinal changes associated with glacio-isostatic adjustment.

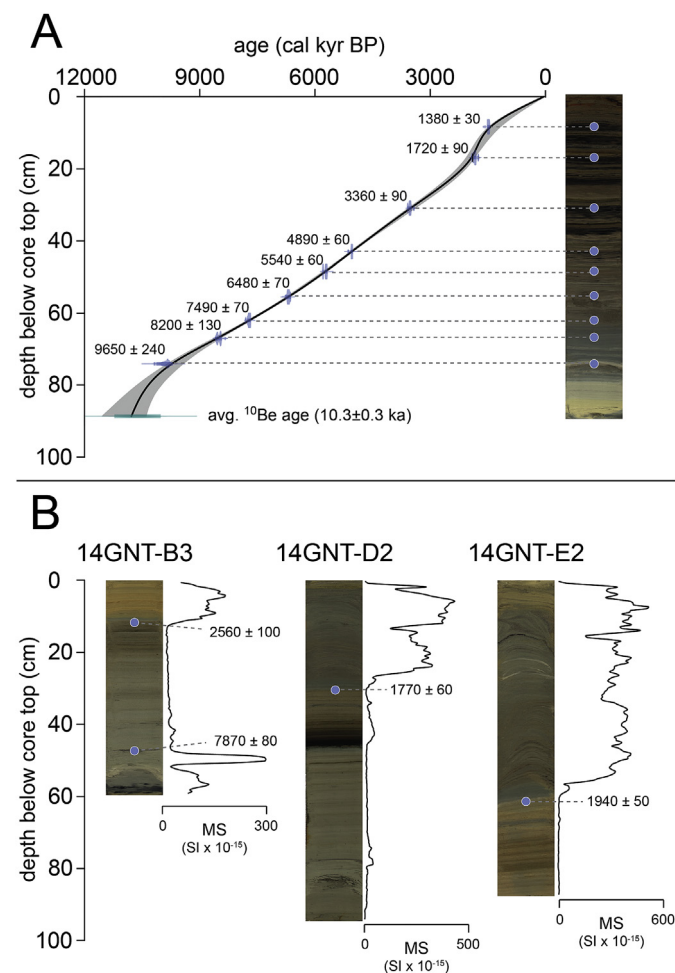


Fig. 6. Age control and stratigraphy for sediment cores reported in this study. A) Crash Lake (14CSH-A1) age-depth model. Light gray lines depict 95% confidence intervals for CLAM 2.2 smooth spline function (smoothing value = 0.2). Radiocarbon ages (cal yr BP; blue circles) are reported as the median of the 2σ range \pm half of the 2σ range uncertainty (Table 2). Crash Lake sediment core photograph shown on the right. B) Sediment cores from proglacial Gnat Lake (14GNT-B3, 14GNT-D2 and 14GNT-E2). Radiocarbon ages of bulk sediment samples (blue circles) and magnetic susceptibility (MS) downcore data are shown. (For interpretation of the references to color in this figure legend, the reader is referred to the Web version of this article.)

package. Radiocarbon ages of $\sim 2.6 \pm 0.1$, 1.8 ± 0.1 , and 1.9 ± 0.1 ka, in cores 14GNT-B3, 14GNT-D2, and 14GNT-E2, respectively (Fig. 6; Table 2), provide general constraints on the timing of ice cap re-growth into the Gnat Lake catchment. Because these are maximum age constraints, we interpret the youngest radiocarbon ages (~ 1.9 – 1.8 ka) as the closest constraint on GIC advance into the Gnat Lake catchment. A single radiocarbon age of $\sim 7.8 \pm 0.1$ ka in the lower sediments of core 14GNT-B3 provides a minimum-limiting age for regional deglaciation (Figs. 2, 3 and 6, Table 2).

An 88.5 cm-long sediment core was recovered from Crash Lake at 32.6 m water depth (Table 1). The lowermost unit of the Crash Lake sediment core (14CSH-A1) is composed of finely laminated yellow to gray clayey silt with high MS, density and K/Ti values, and low LOI values (Figs. 6 and 7). The lowermost unit is overlain by a 15 cm-thick gray mineral-rich unit that includes a distinctive light gray ~2.0-cm-thick clayey silt layer at 73.0 cm depth (Fig. 6). The ~2.0-cm-thick light gray layer corresponds to a peak in MS, density and K/Ti values, and a decrease in LOI values (Fig. 7). Alternating black organic-rich sediments and light to dark brown mineral-rich sediments, which result in fluctuations between relatively higher or lower LOI values, respectively (Fig. 7), characterize the overlying unit. A mineral-rich unit composed of sandy silt caps the Crash Lake sediment core.

Bulk sediment samples from 14CSH-A1 yielded nine stratigraphically consistent radiocarbon ages that we use to generate an age-depth model (Fig. 6; Table 2). The lower-most radiocarbon age of $\sim 9.7 \pm 0.2$ ka provides a minimum-limiting age for deglaciation of the site or at least a significant reduction in glacier size (Table 2), which is in general agreement with other radiocarbon ages from the study region (Sudgen, 1972) and ¹⁰Be ages of nearby erratics that average $\sim 10.3 \pm 0.3$ ka (Lesnek and Briner, 2018). Density, MS and K/Ti values steadily decrease while organic matter increases until ~ 6.5 cal yr BP with the exception of a prominent peak in density, MS and K/Ti values at ~ 9.3 cal yr BP (Fig. 7). After ~ 6.5 cal yr BP, Crash Lake sediments become more variable; shifts from dark brown to black organic-rich material to mineral-rich sediments appear episodic, and are superimposed on increasing mineral input (and decreasing organic content) throughout the last ~ 4.5 ka (Fig. 7).

PCA was used to detect patterns of variability that are shared between the Crash Lake sediment variables (e.g., Vasskog et al., 2012; Røthe et al., 2015; Larsen et al., 2017; Schweinsberg et al., 2017). LOI, MS, and density, and XRF elemental data Si, Ca, Mn, Fe, Rb, Sr, and K/Ti are used in the PCA. The first Principal Component (PC1) explains 52% of the total variance, implying that the dataset contains a strong common signal that is reflected by

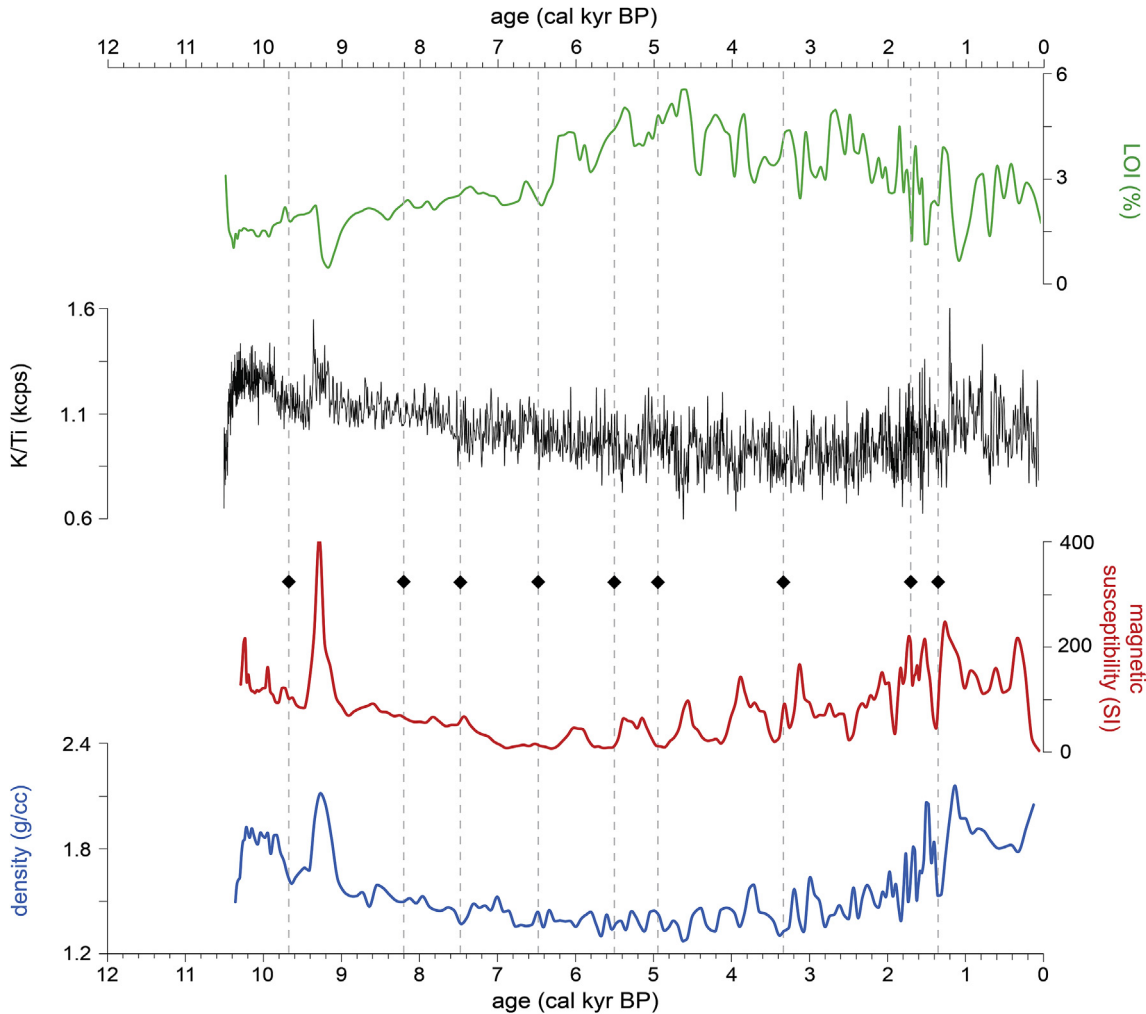


Fig. 7. Downcore data for Crash Lake. Physical parameters include magnetic susceptibility (red curve), density (gray curve) and LOI (green curve). The K/Ti elemental data (black curve) are also shown. Black diamonds denote radiocarbon ages. (For interpretation of the references to color in this figure legend, the reader is referred to the Web version of this article.)

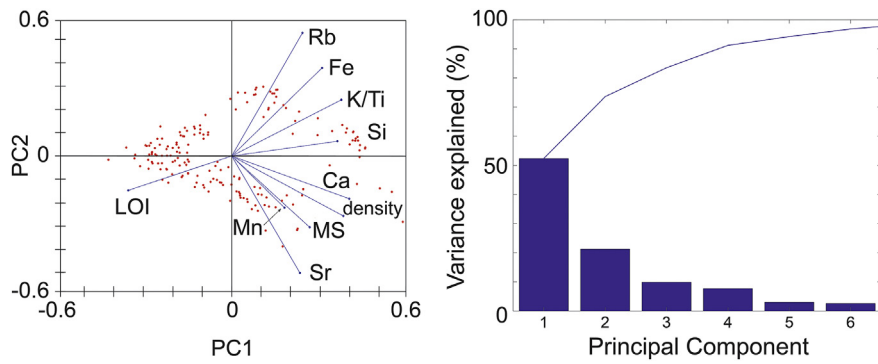


Fig. 8. PCA results for Crash Lake sediment core. (A) Biplot showing first and second Principal Component axes. (B) Scree plot of PCA results.

many of the variables (Fig. 8). Trends in PC1 are similar to those in MS and density, parameters typically used to reconstruct glacier size (e.g., Dahl et al., 2003), justifying the use of PC1 score to infer past fluctuations in local glacier extent through time (Figs. 7 and 10; Balascio et al., 2015; Larsen et al., 2017; Schweinsberg et al., 2017).

Crash Lake PC1 scores reflect mineral sediments present at the sediment core base (Fig. 10). At ~9.3 ka, a layer of mineral-rich

sediment was deposited into the lake; this layer may represent a glacier advance. Following ~9.3 ka, GIC in the study area were steadily retreating until ~4.6 ka, which is correlative with a time in western Greenland described as the thermal maximum (Briner et al., 2016). The Crash Lake record suggests that the onset of Neoglaciation occurred ~4.6 ka, and the subsequent stepwise increases in mineral-rich sediment input (decrease in organic matter

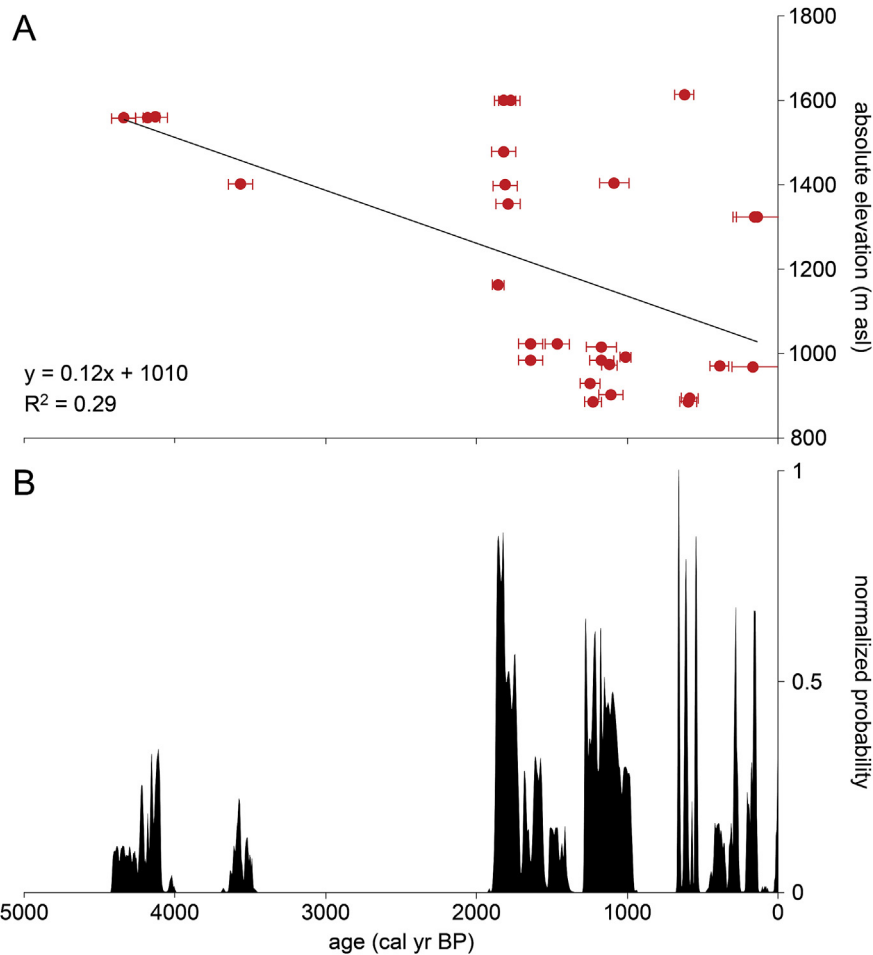


Fig. 9. Calibrated ages of moss samples collected in the Sukkertoppen region. A) The 29 calibrated radiocarbon ages for *in situ* moss in the Sukkertoppen region plotted against the elevation (m asl) of their collection site. Solid line denotes the least squares regression through all data. B) Aggregated PDF of *in situ* moss samples in the Sukkertoppen region (Table 3).

content) after ~4.6 ka suggests that rather than advancing steadily towards their historical extent, Sukkertoppen GIC episodically advanced and retreated at centennial timescales (Fig. 10). Interpreted literally, the PC1 scores suggest that GIC reached their greatest extent in the late Holocene at ~1.5 ka followed by ice expansion between ~1.2 and 1.0 ka and during the LIA (Fig. 10).

5.2. Sukkertoppen moss dataset

Radiocarbon ages of *in situ* moss that recently emerged from beneath receding cold-based ice margins define the pattern and timing of past episodes of snowline lowering that led to ice cap expansion in the late Holocene at the multi-decadal to centennial-scale (e.g., Anderson et al., 2008; Miller et al., 2012, 2013a; b; 2017; Margreth et al., 2014; Miller et al., 2017; Schweinsberg et al., 2017). A total of 34 *in situ* moss samples were dated from 10 independent ice caps with elevations ranging from 668 to 1611 m asl in the study region; six collections are from high-elevation plateaus located between valley glacier outlets on Sukkertoppen Iskappe, seven samples are located on the margin of Qaarajuttoq, and the remaining 21 moss samples were collected from the edges of smaller ice caps throughout the field area (Figs. 2 and 9; Table 3). For comparison with our Crash Lake record and other regional paleoclimate proxies, we generate a summed probability plot using the function in CALIB 7.0 (Fig. 9), and acknowledge the

amplification of some individual peaks through the calibration process (Chiverrell et al., 2011; Williams, 2012; Armit et al., 2013; Margreth et al., 2014). Replicate samples (14GROV-47A, -47B, -47C), 14GROV-39 (grass), and samples with radiocarbon ages within the atmospheric bomb-testing era (i.e., $F_m > 1$; 14GROV-14A, -14B-, -14C) are omitted from the summed probability plot.

Excluding the replicate ($n = 3$) and modern ($n = 3$) samples, moss samples collected at elevations between 880 and 1610 m asl yield calibrated ages ranging from ~4.3 to 0.2 ka (Fig. 9; Table 3). The oldest grouping is defined by three radiocarbon ages ranging from ~4.3 to 4.1 ka, followed by a single radiocarbon age at ~3.6 ka. Following a ~1500 year gap, the remaining age clusters occur in the last 2000 years. The largest number of radiocarbon ages ($n = 9$) delineate a cluster ranging from ~1.9 to 1.5 ka, and are well-distributed throughout an elevation range of 980–1600 m asl, implying widespread ice expansion across a large elevation range in the field area. A second major grouping consisting of eight radiocarbon ages falls between ~1.3 and 1.0 ka. Contrary to the older clusters, the majority of radiocarbon ages in this cluster are from a small elevation range (~850–1000 m asl) despite covering 10 different ice caps. The youngest and most variable age cluster (likely due to calibration artifacts) includes seven radiocarbon ages that range between ~0.7 and 0.2 ka, and display the largest range in sample site elevations (Fig. 9).

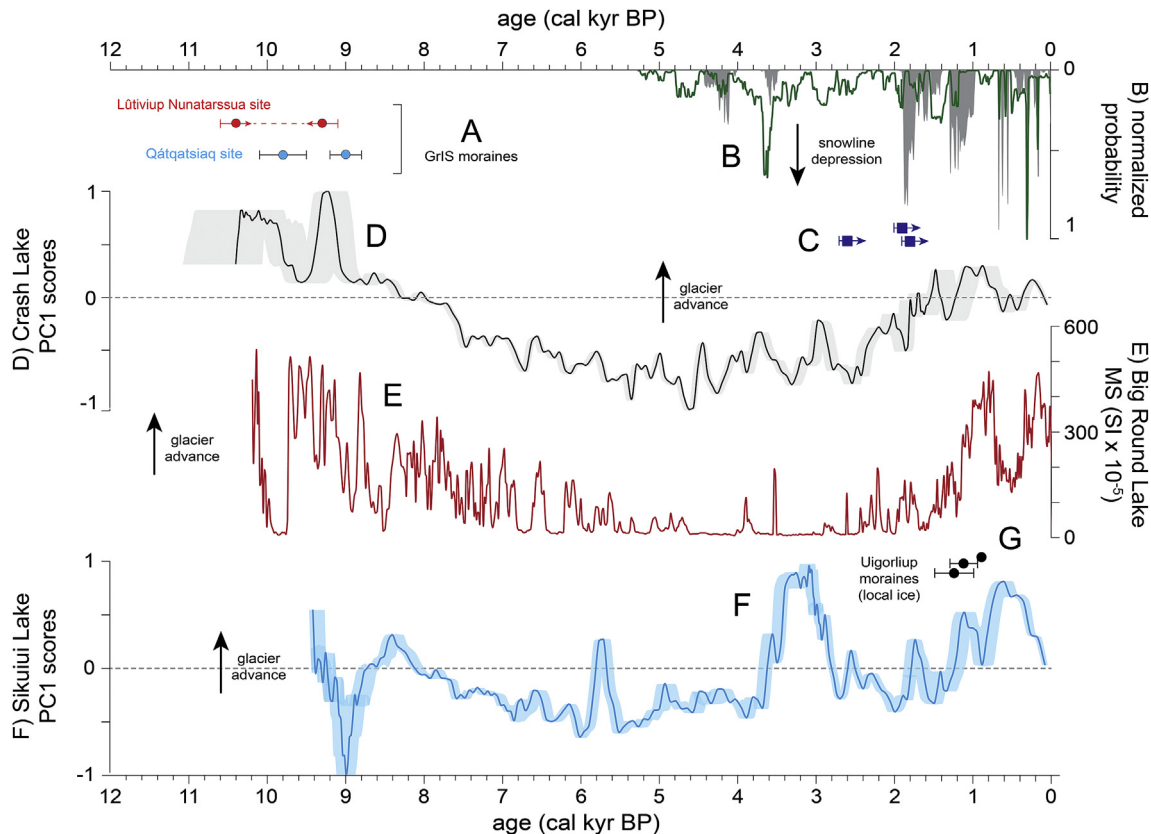


Fig. 10. Glacier-size proxy records from the Sukkertoppen region compared with other regional datasets. A) Moraines dated in the Sukkertoppen field area ([Lesnek and Briner, 2018](#)). B) Aggregated distributions of radiocarbon ages of mosses from the Disko Bugt region, West Greenland ($n = 54$, green curve; [Schweinsberg et al., 2017](#)), and this study ($n = 29$; gray shading). C) Bulk sediment radiocarbon ages from Gnat Lake cores (median age $\pm 2\sigma$ uncertainty). D) PC1 scores from Crash Lake (gray shading = 95% age uncertainty). E) MS record from Big Round Lake, Baffin Island, Arctic Canada ([Thomas et al., 2010](#)). F) PC1 scores from Sikuliui Lake (blue shading = 95% age uncertainty; [Schweinsberg et al., 2017](#)). G) Mean ages (black circles) and 1σ uncertainty of Uigorliup moraines ([Young et al., 2015](#)). (For interpretation of the references to color in this figure legend, the reader is referred to the Web version of this article.)

We collected additional samples to test some of the primary assumptions of the method ([Miller et al., 2013a; b; Margreth et al., 2014](#)). At one site, we dated four moss samples (14GROV-47A through 14GROV-47D; [Table 3](#)) from different tundra patches within 200 m of each other to test the possibility that the entombed moss was buried during multiple episodes of snowline lowering. All four samples yielded indistinguishable radiocarbon ages within 2σ uncertainty, supporting the interpretation that radiocarbon ages of rooted mosses represent a single episode of ice cap expansion ([Anderson et al., 2008; Miller et al., 2013a; b; Margreth et al., 2014; Schweinsberg et al., 2017](#)). There have also been concerns about the rapid recolonization of relict moss patches by modern regrowth and regeneration from dormant stem buds ([Lowell et al., 2013; La Farge et al., 2013](#)), both of which would compromise the radiocarbon inventories that would otherwise reflect their date-of-burial beneath expanding ice caps ([Miller et al., 2013b](#)). Previous studies indicated that if mosses avoid erosion and persist on the landscape for ~2–3 years, they often exhibit noticeable new growth ([Miller et al., 2013b](#)). Alternatively, in settings where running water is at minimum and recolonization is inhibited due to the absence of soil, dead moss can be preserved hundreds of meters beyond current ice margins ([Miller et al., 2017](#)). To investigate the preservation and/or possibility of new growth in our field area, we radiocarbon dated three moss samples (14GROV-14A, -14B, -14C) adjacent to modern mosses and located just outside of the LIA ice limit that appeared dead (i.e., no evidence of life or regrowth). Although the geomorphic setting suggested the samples had remained on the landscape

for many years, the samples yielded modern ($F_m > 1$) radiocarbon activity ([Table 3](#)). Lastly, we dated a moss (*Polytrichastrum alpinum*; 14GROV-38) and grass (*Poaceae indet.*; 14GROV-39) pair recently exhumed at the ice edge to determine if different plant types yield dissimilar radiocarbon ages. 14GROV-38 and 14GROV-39 returned ages of 370 ± 60 and 150 ± 150 cal yr BP, respectively. The large uncertainty associated with 14GROV-39 makes it difficult to address the age difference between the two plant types.

5.3. ^{10}Be dating

The ^{10}Be age of 14GROR-24 suggests that deglaciation of a small local ice cap south of Qaarajuttoq occurred at $\sim 9.0 \pm 0.3$ ka ([Fig. 2](#); [Table 4](#)). Boulders perched on bedrock, near ice cap margins and located outboard of the early Holocene moraine belts, average 10.3 ± 0.3 ka ($n = 6$; [Lesnek and Briner, 2018](#)), indicating that deglaciation of local ice at higher elevations may have occurred up to 1000 years later than retreat of the GrIS from the study region. Collectively, the ten ^{10}Be ages from erratics in the field area indicate that deglaciation in the vicinity of the studied ice caps occurred sometime between ~10 and 9 ka.

5.4. *In situ* ^{14}C measurements and modeled exposure-burial scenarios

To reconstruct possible exposure-burial histories during the Holocene, we couple the measured *in situ* ^{14}C concentrations of

bedrock with the radiocarbon age from the adjacent moss sample to constrain the cumulative duration of ice cover since deglaciation for six sites in the Sukkertoppen region. Each site requires a different (but unknown) combination of exposure and burial to yield the measured *in situ* ^{14}C inventory. To generate plausible scenarios, we use the following set of boundary conditions in our models: 1) The most recent period of burial (ice cover) is constrained by the radiocarbon age of the adjacent moss sample, which identifies how long the site was ice covered immediately prior to the year of collection (C.E. 2014). 2) If the period of ice cover constrained by the moss radiocarbon age is not of sufficient duration to result in the measured *in situ* ^{14}C inventory, earlier episodes of burial are required. We constrain the duration of earlier burial by subtracting the interval of recent ice cover from the total duration of burial constrained by the *in situ* ^{14}C concentration. 3) For those sites that require additional periods of ice cover, the timing of prior burial is guided by older clusters in the Sukkertoppen moss dataset, which provide an independent control for the possible times of earlier ice expansion. 4) The precise timing of deglaciation at each individual site is unknown. Nearby ^{10}Be ages (Lesnek and Briner, 2018) suggest that deglaciation occurred ~10 ka, which we use to constrain the timing of deglaciation for sites that require more than one interval of burial. In contrast, some sites require only the most recent period of burial to achieve the measured *in situ* ^{14}C inventory. In these cases, our models solve for the onset of deglaciation at that particular site as a function of ice thickness.

We do not know the ice thickness history at each of our sites, and acknowledge that there can be partial *in situ* ^{14}C production (due to muonic production) during intervals of burial with ice thicknesses <100 m (e.g., Lupker et al., 2015; Hippe, 2017). To explore this issue, we use a variety of ice thicknesses in our modeled scenarios. In these cases, ice thickness remains constant during each individual burial episode, and we do not account for the thickening and thinning of ice as it covers and uncovers our sample locations. Therefore, our modeled burial durations are interpreted as minima, and the corresponding exposure durations are maxima.

For three of our six samples, the *in situ* ^{14}C inventory and the adjacent moss radiocarbon age are compatible with one period of burial. Samples 14GROR-03, 14GROR-16 and 14GROR-41 do not require more ice cover than the most recent episode constrained by the paired moss age (Fig. 11B, D, and 11F). For samples 14GROR-03 and 14GROR-41, our model suggests deglaciation occurred as early as ~12.5 and 11.1 ka for 100 m-thick ice cover, respectively, and as late as ~11.8 and 10.9 ka for an ice thickness of 20 m, respectively (Fig. 11B and F). Both of these sample sites are high elevation nunataks within the Qaarajuttoq ice cap (Fig. 2), and may have protruded through thinning ice earlier than the other study sites. Regardless of ice thickness, our models suggest that these sites deglaciated earlier than ages from lower elevations in our field area (Lesnek and Briner, 2018). The exposure-burial scenario for site 14GROR-16 suggests that with continuous ice cover for the past ~4.4 ka an onset of deglaciation occurred sometime between ~9.8 and 8.9 ka for ice thicknesses of 100 to 20 m (Fig. 11D).

For the other three samples, the measured *in situ* ^{14}C inventories indicate that multiple episodes of burial are required following deglaciation at ~10 ka. Considering the guidelines and assumptions described above, we solve for exposure-burial scenarios at each site with ice cover ranging from 20 to 100 m thick during intervals of burial (Fig. 11A, C and 11E). Our models suggest that if ice completely shielded the 14GROR-02 site (100 m thick) that the cumulative duration of burial earlier in the Holocene would be ~2920 years (Fig. 11A). If ice was 20 m thick during burial intervals, an additional 300 years is needed to meet the measured *in situ* ^{14}C concentration. Similarly, an additional 120–320 years of burial is

necessary for ice thicknesses of 35 and 20 m, respectively, than for 100 m-thick ice cover for sample 14GROR-23 (Fig. 11E). Using the larger dataset of radiocarbon-dated moss from the study region, we suggest that ice cover occurred sometime between ~4.4 and 2.2 and 4.4–2.8 ka for 14GROR-02 and 14GROR-23, respectively (Fig. 11A and C). We find that these periods of burial, combined with the most recent episode known from the moss radiocarbon age and deglaciation at 10 ka, result in the measured ^{14}C inventories for these sample sites.

To achieve the measured ^{14}C inventory for 14GROR-15, ice must cover the site for ~1600 (100 m) to 2000 (20 m) years in addition to continuous ice cover for the past ~3.6 ka (moss radiocarbon age). This results in a cumulative burial duration of up to 5.6 ka (with 20 m-thick ice cover). Therefore, the earlier episode of ice cap occupation at the 14GROR-15 site may have occurred prior to 5 ka under the model conditions described above (Fig. 11C). Alternatively, the onset of the earlier burial interval can be shifted to after 5 ka if near-complete to complete shielding occurs (ice thicknesses >50 m) and a later deglaciation takes place at ~9 ka.

6. Discussion

6.1. Fluctuations of glaciers in the Baffin Bay region

Here, we summarize our GIC reconstructions from the Sukkertoppen region and compare them with records of GIC and GrIS margin fluctuations from elsewhere around Greenland and Baffin Bay. Following regional deglaciation of the area ~10 ka (Lesnek and Briner, 2018), a brief interval of increased mineral-rich input shows that GIC retreat during the early Holocene may have been interrupted by an episode of glacier advance at ~9 ka, coeval with the deposition of nearby ice sheet moraines (Qáqtatsiaq site; Lesnek and Briner, 2018) and the Marrait moraine near Disko Bugt, which was dated to 9.2 ka (Young et al., 2011, 2013b). This potential synchronicity of local glacier and GrIS margin behavior would suggest that both the GrIS and GIC in West Greenland responded to centennial-scale climatic perturbations during the early Holocene. Additionally, an interval of high MS values from sediments in Big Round Lake on Baffin Island, Arctic Canada (Thomas et al., 2010), implies glacier growth between ~9.7 and 9.2 ka that is coeval with our local glacier reconstruction (Fig. 10).

Following a potential ice advance at ~9 ka, Sukkertoppen glaciers steadily retreated and reached their minimum Holocene extent ~5 ka, inferred from low mineralogenic content and PC1 scores, and relatively higher LOI values in the Crash Lake sediments (Figs. 7 and 10). It is likely that the sediments ~5 ka reflect a period where GIC in the Crash Lake catchment were smaller than today, or completely absent. The timing of restricted ice documented in our record overlaps with some records of the regional thermal maximum (e.g., Andresen and Leng, 2004; Axford et al., 2009; Briner et al., 2016), and with the absence of local ice in catchments studied in southeast Greenland (~7.8–4.1 ka; Balascio et al., 2015), West Greenland (~7.9–5.5 ka; Larsen et al., 2017) and on Baffin Island (~6–3 ka; Thomas et al., 2010). Overall, a remarkable similarity exists between the inferred glacier size records developed from Crash and Big Round lakes (Fig. 10). For example, both reconstructions reveal decreasing mineral input between ~9 and ~5 ka, followed by increasing mineral input through the past few millennia. This may suggest that local glacier behavior was modulated by a common climate forcing in the Baffin Bay region throughout the Holocene (Fig. 10).

Radiocarbon ages of *in situ* mosses reflect the earliest evidence of Neoglacial snowline lowering at ~4.3 ka that is generally coincident with the onset of glacier growth (increasing PC1 scores) recorded in Crash Lake at ~4.6 ka (Fig. 10). The onset of Neoglacial

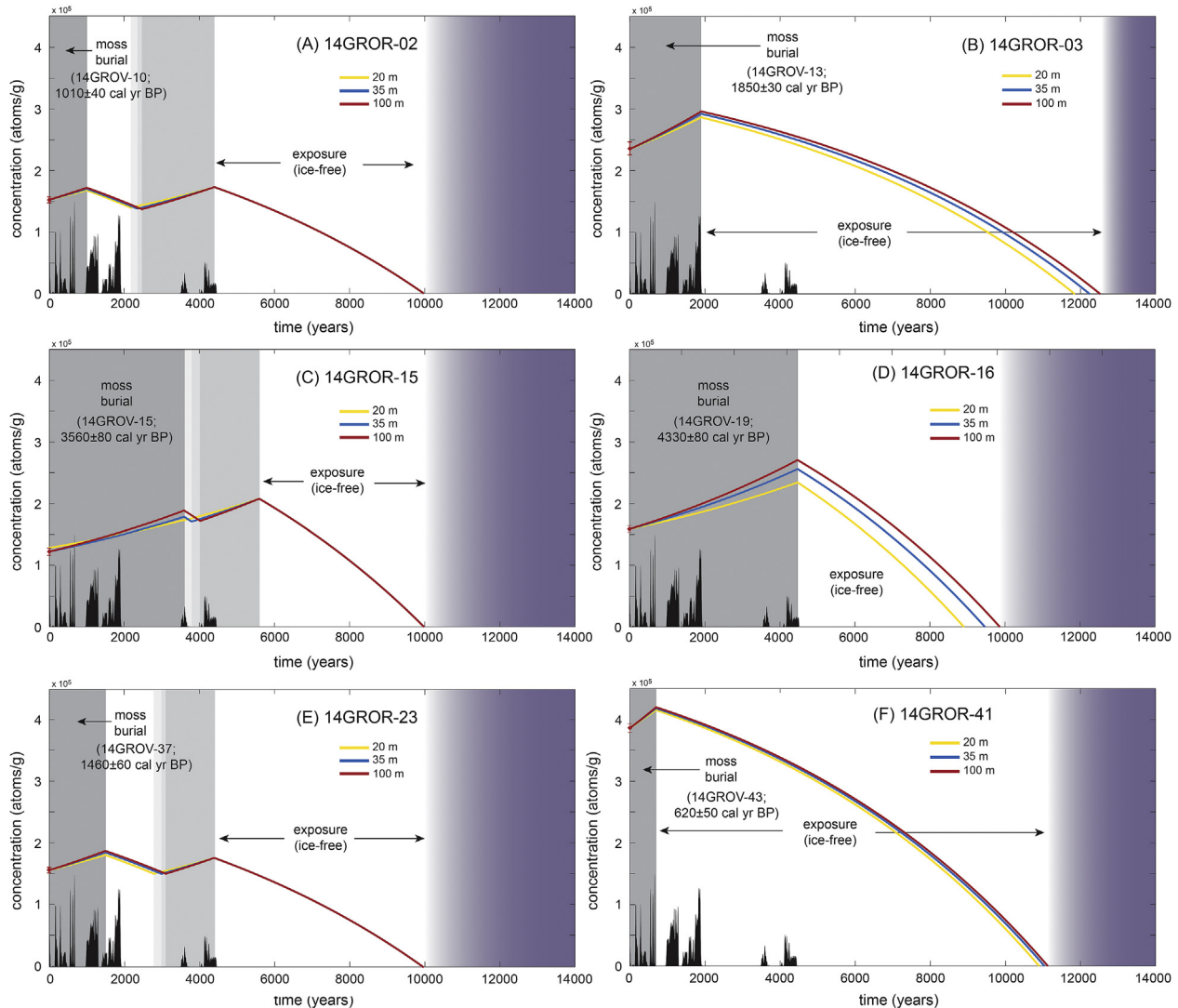


Fig. 11. Modeled exposure-burial scenarios based on *in situ* ^{14}C inventories. White sections denote post-glacial ice-free periods (times of exposure) while gray bars indicate intervals of Holocene ice cover. Purple bars reflect burial prior to deglaciation of the site. The most recent period of ice cover is constrained by the paired moss sample (darkest gray bar). Additional gray bars denote earlier periods of ice cover; the duration of ice cover is dependent on ice thickness. The timing of earlier burial episodes is constrained by the Sukkertoppen moss dataset (aggregated PDF shown at bottom in black). Red diamonds at time zero mark the measured *in situ* ^{14}C concentration and uncertainty for each bedrock sample. Colored lines represent each sample site's exposure-burial history with varying ice thickness. We note that the modeled ages represent the minimized solution for each sample's measured concentration. (For interpretation of the references to color in this figure legend, the reader is referred to the Web version of this article.)

cooling in the Sukkertoppen area is consistent with regrowth of local glaciers in central West Greenland at ~5 ka (Schweinsberg et al., 2017) and elsewhere in southwestern Greenland at ~5.5 ka (Larsen et al., 2017). Curiously, the interval of significant glacier expansion recorded in Sikuli Lake sediments and moss radiocarbon ages at ~3.7 ka (Fig. 10; Schweinsberg et al., 2017), and from proglacial lakes in Kobbefjord between 3.6 and 3.5 ka (Fig. 1; Larsen et al., 2017), is not well-expressed in the Sukkertoppen moss series, with the exception of a single radiocarbon age of 3.6 ka (Fig. 10; Schweinsberg et al., 2017). However, intervals of glacier advance recorded in Crash Lake sediments at ~3.7 and 2.9 ka appear to correspond with episodes of snowline lowering in other regional GIC reconstructions from Greenland (Balascio et al., 2015; Larsen et al., 2017; Schweinsberg et al., 2017). The absence of moss ages ~3.7 ka may be attributed to the relatively small size of our dataset ($n = 29$), particularly for the interval preceding the last ~2 ka. However, we argue that with 24 out of 29 collections dating to the last ~2 ka, the pattern in the latest Holocene is fairly robust.

Our glacier-size proxies from the Sukkertoppen region reveal centennial-scale episodes of ice cap advance coeval with changes in local glacier behavior from regional datasets since ~2 ka (Fig. 10). The past two millennia exhibit stepwise glacier growth including three to four advance and retreat cycles superimposed on an overall summer cooling trend that is reflected in both the sediment and moss records from western Greenland and Baffin Island (Thomas et al., 2010; Miller et al., 2013a; b; Schweinsberg et al., 2017). Intensified ice expansion denoted by the largest age cluster in the moss series and increasing Crash Lake PC1 scores marks renewed ice growth in response to snowline depression at ~1.8 ka. This period of glacier expansion is recorded in West Greenland and Baffin Island proglacial lakes (Thomas et al., 2010; Schweinsberg et al., 2017), and is consistent with widespread glacier advances dating between ~2 and 1 ka in the North Atlantic region (Bakke et al., 2010; Miller et al., 2013a; b; Larsen et al., 2014; Levy et al., 2014; Margreth et al., 2014; Balascio et al., 2015; Solomina et al., 2015; Miller et al., 2017). A second glacier advance occurs

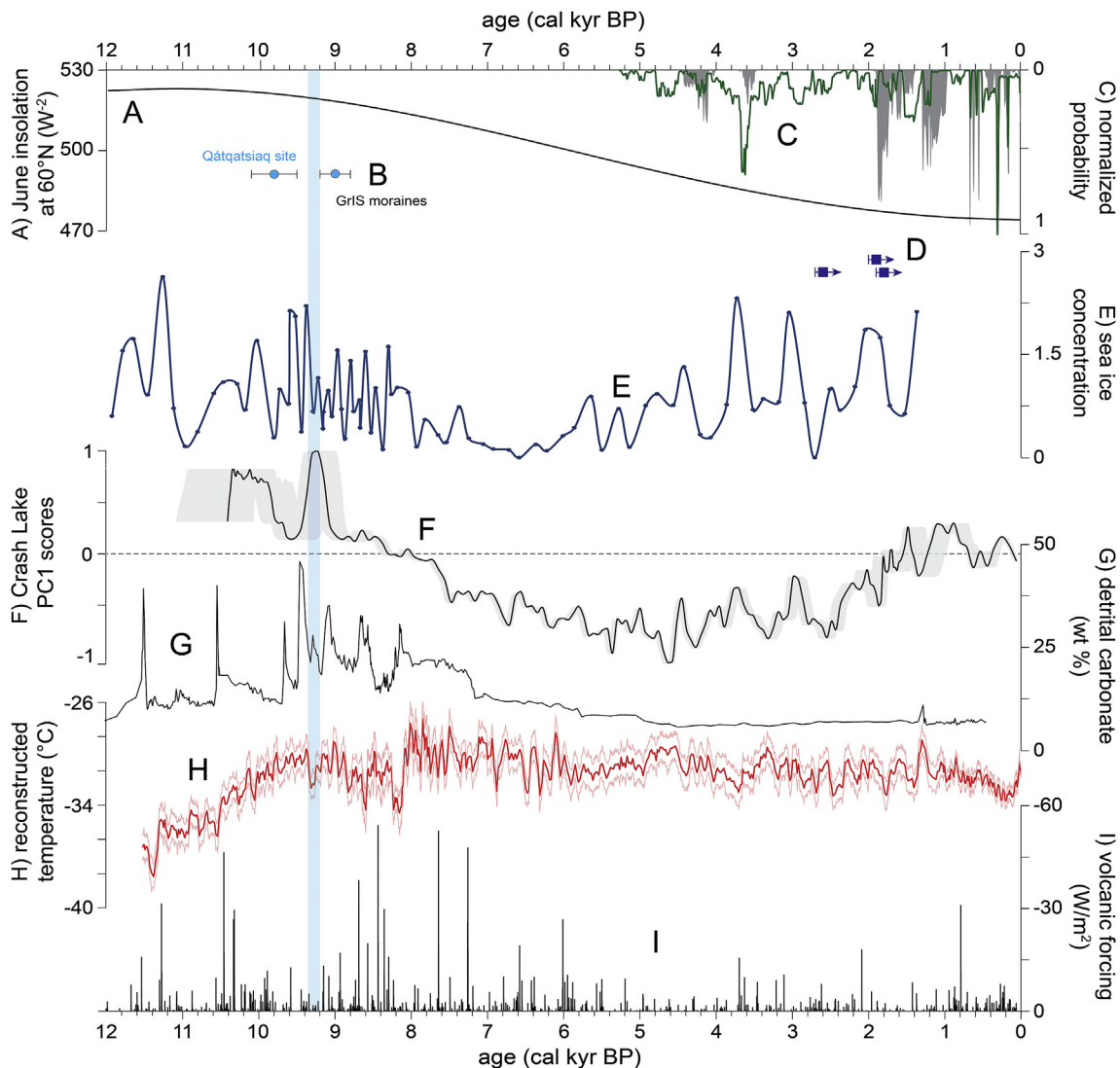


Fig. 12. Glacier-size proxy records from the Sukkertoppen region compared with possible climate forcings during the Holocene. A) June insolation at 60 °N (Berger and Loutre, 1991). B) GrIS moraines dated in the Sukkertoppen field area (Lesnek and Briner, 2018). C) Aggregated distributions of radiocarbon ages of mosses from West Greenland ($n = 54$, green curve; Schweinsberg et al., 2017) and this study ($n = 29$, gray shading). D) Maximum radiocarbon ages for ice advance from Gnat Lake. E) Reconstructed sea ice concentration based on dinocyst data from core HU013 in the Labrador Sea (de Vernal et al., 2013). F) PC1 scores from Crash Lake (gray shading = 95% age uncertainty). G) Detrital carbonate content of marine sediment core MD99-2236 on the Labrador Shelf (Jennings et al., 2015). H) GISP2 temperature (red line) with 2σ error (Kobashi et al., 2017). I) Volcanic forcing generated from sulfate concentrations in GISP2 (Kobashi et al., 2017). Vertical blue denotes the 9.3 ka event (~9350–9200 years ago; Vinther et al., 2006; Rasmussen et al., 2007; Fleitmann et al., 2008). (For interpretation of the references to color in this figure legend, the reader is referred to the Web version of this article.)

between ~1.2 and 1.0 ka, and is correlative with the deposition of late Holocene moraines on Nuussuaq and Baffin Island (Young et al., 2015). The most recent age cluster is coincident with increasing glacier extent during the LIA at ~0.7 cal yr BP, a time when numerous GrIS margin advances have been documented (e.g., Weidick and Bennike, 2007).

6.2. Climate forcing

In this section, we examine possible mechanisms and climate forcings that may have influenced local glacier behavior during the Holocene in southwestern Greenland. The evidence from Crash Lake for a glacier advance at ~9 ka is indistinguishable from the timing of moraine deposition in the study area (Lesnek and Briner, 2018) and in the Disko Bugt region (Young et al., 2011, 2013b). This implies a synchronous response of local glaciers and the western GrIS margin to centennial-scale climate variations at this time.

Previous studies of GrIS margin change proposed that hemispheric cooling episodes in the early Holocene were driven by large pulses of freshwater from the Laurentide Ice Sheet into the North Atlantic, which led to cooling in Baffin Bay (Young et al., 2011, 2013b; Lesnek and Briner, 2018). The record of freshwater forcing events from the Laurentide Ice Sheet (Jennings et al., 2015) also includes a detrital carbonate peak ~10.5 cal ka BP, which has been tied to local glacier moraines on Nuussuaq (Fig. 1; O'Hara et al., 2017). This event may relate to the older of two moraines dated by Lesnek and Briner (2018) and the basal mineral-rich sediments in Crash Lake.

The 8.2 ka cooling event registered in marine and terrestrial archives around Greenland and Baffin Bay (Alley and Ágústsdóttir, 2005; Vinther et al., 2006; Young et al., 2011, 2013b; Jennings et al., 2015) is not prominently expressed in the Crash Lake sediments nor in the GrIS moraine record in the study area (Lesnek and Briner, 2018). On the other hand, the Umivit-Keglen GrIS moraines in the Kangerlussuaq region date to ~8.2 ka (Winsor et al., 2015a).

Thus, it is possible that GrIS moraines dating to that interval, if any, are located farther east in the Sukkertoppen area. PC1 scores in Crash Lake remain slightly elevated until after ~8 ka, suggesting that there may have been a small amount of lingering ice in the Crash Lake catchment until that time. Alternatively, the regional snowline had risen out of Crash Lake's catchment before ~8.2 ka.

It is also possible that early Holocene ice cap fluctuations were influenced by large and frequent volcanic eruptions that led to summer cooling and affected ocean surface conditions and sea-ice formation (Fig. 12; de Vernal et al., 2013; Kobashi et al., 2017). Although we postulate that the ~9 ka glacier advance in southwest Greenland may correlate with abrupt cooling in response to freshwater forcing, it is plausible that sustained volcanic eruptions throughout the early Holocene would have reduced temperatures (Kobashi et al., 2017) and led to increased glacier mass balance. It is difficult to assess the importance of volcanic activity and freshwater forcing on early Holocene Sukkertoppen GIC fluctuations. Moreover, fluctuations in solar activity has been linked to centennial temperature change in Greenland (Adolphi et al., 2014; Kobashi et al., 2015), implying that abrupt or episodic climate change events, and associated impacts on the cryosphere, during the Holocene may result from changes in several forcings (volcanic, solar, and meltwater inputs).

We document a progressive increase in Sukkertoppen GIC extent after ~4.6 ka that is consistent with declining Northern Hemisphere summer insolation. However, the oscillatory and stepwise increases in minerogenic input to Crash Lake and the distinct periods of snowline lowering suggest that centennial-scale climate variability influenced glacier fluctuations (Figs. 10 and 12). Studies of local glacier behavior in Greenland and around the North Atlantic region have suggested that intervals of snowline depression and glacier advance may be linked to colder oceanic conditions and the associated decline in terrestrial temperatures (e.g., Geirsdóttir et al., 2013; Larsen et al., 2012; Balascio et al., 2015; Schweinsberg et al., 2017). Variability in solar irradiance and explosive volcanism may also have affected past climate on multidecadal timescales, and may have led to conditions favorable for ice cap expansion. For example, volcanic eruption-induced cooling maintained by strong sea-ice/ocean feedbacks may have triggered late Holocene centennial cooling in the Northern Hemisphere (Miller et al., 2012; Sigl et al., 2015), resulting in snowline depression and glacier growth during the LIA and other cold intervals within the last millennium (Anderson et al., 2008; Miller et al., 2012, 2017; Geirsdóttir et al., 2013). More recently, volcanism has been suggested to exhibit a strong influence on centennial to millennial-scale temperature change throughout the Holocene record in Greenland (Kobashi et al., 2017), implying that volcanic impacts on the Northern Hemisphere climate system were not limited to the recent millennia and that cold intervals throughout the Holocene, such as cooling between ~9 and 8 ka, may be attributable in part to volcanic origin.

We find that reconstructed Greenland temperatures in GISP2 (Kobashi et al., 2017) are broadly consistent with our glacier-size proxy records from Sukkertoppen since ~4.0 ka, suggesting that fluctuations in GIC extents in this region are tightly coupled to Holocene atmospheric temperatures (Fig. 12). Persistent summer cooling and local glacier expansion between ~3.7 and 3.4 ka (Balascio et al., 2015; Larsen et al., 2017; Schweinsberg et al., 2017) appear to correlate with a decrease in GISP2 temperatures and a period of intensified volcanic activity between ~3.8 and 3.5 cal ka BP (Fig. 12; Kobashi et al., 2017). Similarly, other local glacier advances in our study area and elsewhere in Greenland documented at ~2.9, ~1.8 and ~0.7 ka (Balascio et al., 2015; Larsen et al., 2017; Schweinsberg et al., 2017) are broadly consistent with relatively lower GISP2 temperatures, higher concentrations of sea ice, and

occur during or following intervals of volcanic activity (Fig. 12). These correlations suggest that episodes of snowline depression and ice advance in the Sukkertoppen region during the past 4.0 ka may be associated with lower temperatures and positive sea-ice/ocean feedbacks that may have been triggered by episodes of repeated explosive volcanism. Model simulations indicate that cold periods of centennial to millennial duration can be produced by a series of consecutive large volcanic eruptions, and that lower temperatures can persist at high northern latitudes for a century or more long after volcanic aerosols are removed from the atmosphere (Schneider et al., 2009; Miller et al., 2012; Sigl et al., 2015; Kobashi et al., 2017). Furthermore, sea-ice expansion following volcanic eruptions can lead to freshening and vertical stratification of the North Atlantic subpolar gyre, reducing open ocean convection and thus weakening the Atlantic meridional overturning circulation (Zhong et al., 2011; Miller et al., 2012). Thus, we speculate that volcanic activity throughout the past ~4.0 ka, although less frequent and intense than in the early Holocene and during the LIA, may have led to centennial-scale variability imprinted on overall glacier size due to insolation forcing. The growing body of evidence for regional synchronicity and widespread glacier advances corresponding to centennial-scale cold periods during the late Holocene in the North Atlantic region (e.g., Solomina et al., 2015) points to forcing mechanisms operating on a regional and/or hemispheric scale.

7. Conclusions

Our multi-proxy glacier-size reconstruction illustrates that GIC in the Sukkertoppen Iskappe area experienced centennial-scale variations superimposed on the millennial-scale insolation-driven net increase in glacier size during the Holocene. The Crash Lake record reveals an ice cap advance at ~9 ka that is coeval with GrIS moraines in the study area (Lesnek and Briner, 2018) and in the Disko Bugt region (Young et al., 2011, 2013b), implying that both the western GrIS margin and GIC responded synchronously to a centennial-scale climatic perturbation at this time. The glacier fluctuations at ~9 ka were concurrent with a hypothesized freshwater pulse stemming from the Laurentide Ice Sheet (Yu et al., 2010; Jennings et al., 2015), suggesting that freshwater forcing likely influenced early Holocene climate in Baffin Bay (e.g., Young et al., 2011, 2013b).

The Sukkertoppen moss chronology reveals the onset of snowline lowering in the field area at ~4.3 ka followed by intervals of summer cooling and ice cap expansion at ~1.8, 1.2 and 0.7 ka. This pattern of glacier change also recorded by the Crash and Gnat lake sediment records, which document increasing glacier size in-step with cooling episodes documented in the moss chronology. In addition, the Crash Lake sediment sequence records intervals of increasing glacier extent not captured by the moss dataset, including episodes of GIC expansion at ~3.7 and 3.0 ka that are registered in other glacier reconstructions in Greenland and the North Atlantic region (e.g., Balascio et al., 2015; Larsen et al., 2017; Miller et al., 2017; Schweinsberg et al., 2017).

In situ ^{14}C inventories in bedrock surfaces allow for the quantification of complex Holocene ice-cover histories in the Sukkertoppen region. Although the interval of burial constrained by the paired moss radiocarbon ages is variable between sites, our modeled exposure-burial scenarios indicate that earlier burial episodes were of comparable duration and are compatible with other regional climate proxies for ice cap expansion. Our models also illustrate that deglaciation was likely variable across the field area, and that the timing of local deglaciation is a function of geologic setting.

The record of GIC fluctuations presented here benefits from integrating several different methods to characterize glacier

variability during the Holocene. While each technique provides valuable information on glacier change when used individually, a multi-proxy approach delivers independent lines of evidence that help to evaluate and resolve ambiguities with interpreting each proxy record alone. Proglacial lake sediments can preserve continuous high-resolution records of Holocene GIC fluctuations, but sediment records also include non-glacial sediment inputs and/or within-lake processes that often complicate identification of the true glacial signal. Although the composite series of *in situ* moss radiocarbon ages securely dates the onset of glacier expansion across the region (Miller et al., 2012, 2013a; b; Margreth et al., 2014; Schweinsberg et al., 2017), individual moss radiocarbon ages constrain only the most recent episode of ice cap growth at the collection site (Anderson et al., 2008; Miller et al., 2013a; b; Margreth et al., 2014; Schweinsberg et al., 2017). Furthermore, this method has been met with multiple interpretations, particularly with respect to the collection protocols employed (Miller et al., 2013b). Measured *in situ* ^{14}C inventories estimate the sum of post-deglaciation ice cover; however, identifying when burial episodes occurred requires additional constraints from regional proxy data (Miller et al., 2006; Anderson et al., 2008).

Although each geochronological approach described above has limitations, each proxy complements another when combined. For example, the regional moss distribution and nearby lake sediment records provide insight into the timing and duration of previous GIC expansion episodes prior to the most recent period of burial known from the individual paired moss sample. The merging of moss radiocarbon ages with *in situ* ^{14}C concentrations therefore builds an inventory of the total duration of Holocene ice cover, constrain the most recent episode of burial, and utilizes regional proxy data developed in this study to better quantify complex Holocene ice cover histories across the Sukkertoppen Iskappe area. *In situ* ^{14}C also provides the required level of testing to confirm the continuous burial of the paired radiocarbon-dated moss sample since ice covered the site (e.g., Miller et al., 2013a; b). The *in situ* moss chronology also serves as an independent assessment of glacier growth, thus aiding in the identification of the primary glacial signal in the sediment sequences. ^{10}Be -dating of erratics (this study; Lesnek and Briner, 2018) in our study region is a critical component because ^{10}Be ages provide constraints on the timing of local deglaciation, and provides an essential boundary condition in our exposure-burial models. Collectively, our multi-proxy reconstruction emphasizes that using a suite of techniques results in a more complete understanding of spatio-temporal GIC change, thus providing a more comprehensive view of regional GIC behavior in Southwest Greenland.

Acknowledgements

We would like to thank CH2M Hill Polar Field services for logistical support and the United States 109th Air Lift Wing Air National Guard. We are grateful to PolarTREC for supporting Christina Ciarametaro for research opportunities on Greenland. We thank A. Lesnek for field assistance, S. Cronauer, S. Clements, and C. Sbarra for contributions to lab work in the University at Buffalo Cosmogenic Isotope Laboratory, and C. Beel and B. Goehring for assistance with lab work at Purdue University and in PRIME Lab. Two anonymous reviewer's comments strengthened this manuscript. This research was supported by National Science Foundation grant ARC-1204005.

Appendix A. Supplementary data

Supplementary data related to this article can be found at <https://doi.org/10.1016/j.quascirev.2018.06.014>.

References

- Abbot, M.B., Stafford, T.W., 1996. Radiocarbon geochemistry of modern and ancient arctic lake systems, Baffin Island, Canada. *Quat. Res.* 45, 300–311.
- Adolphi, F., Muscheler, R., Svensson, A., Aldahan, A., Possnert, G., Beer, J., Sjolte, J., Björck, S., Matthes, K., Thiéblemont, R., 2014. Persistent link between solar activity and Greenland climate during the Last Glacial Maximum. *Nat. Geosci.* 7, 662–666.
- Alley, R.B., Ágústsdóttir, A.M., 2005. The 8k event: cause and consequences of a major Holocene abrupt climate change. *Quat. Sci. Rev.* 24, 1123–1149. <https://doi.org/10.1016/j.quascirev.2004.12.004>.
- Andresen, N.J., Leng, M.J., 2004. Increased aridity during the early Holocene in West Greenland inferred from stable isotopes in laminated-lake sediments. *Quat. Sci. Rev.* 23, 841–849.
- Anderson, R.K., Miller, G.H., Briner, J.P., Lifton, N.A., DeVogel, S.B., 2008. A millennial perspective on Arctic warming from ^{14}C in quartz and plants emerging from beneath ice caps. *Geophys. Res. Lett.* 35, L01502.
- Armit, I., Swindles, G.T., Becker, K., 2013. From dates to demography in later prehistoric Ireland? Experimental approaches to the meta-analysis of large ^{14}C data-sets. *J. Archaeol. Sci.* 40, 433–438.
- Axford, Y., Briner, J.P., Miller, G.H., Francis, D.R., 2009. Paleoecological evidence for abrupt cold reversals during peak Holocene warmth on Baffin Island, Arctic Canada. *Quat. Res.* 71, 142–149.
- Balascio, N.L., D'Andrea, W.J., Bradley, R.S., 2015. Glacier response to North Atlantic climate variability during the Holocene. *Clim. Past* 11, 1587–1598.
- Balco, G., 2017. Production rate calculations for cosmic-ray-muon-produced ^{10}Be and ^{26}Al benchmarked against geological calibration data. *Quat. Geochronol.* 39, 150–173.
- Bakke, J., Lie, Ø., Nesje, A., Dahl, S.O., Paasche, Ø., 2005. Utilizing physical sediment variability in glacier-fed lakes for continuous glacier reconstructions during the Holocene, northern Folgefonna, western Norway. *Holocene* 15, 161–176. <https://doi.org/10.1191/0959683605hl797rp>.
- Bakke, J., Dahl, S.O., Paasche, Ø., Simonsen, J.R., Kvistvik, B., Bakke, K., Nesje, A., 2010. A complete record of Holocene glacier variability at Austre Okstindbreen, Northern Norway: an integrated approach. *Quat. Sci. Rev.* 29, 1246–1262.
- Beel, C.R., Lifton, N.A., Briner, J.P., Goehring, B.M., 2016. Quaternary evolution and ice sheet history of contrasting landscapes in Uummannaq and Sukkertoppen, western Greenland. *Quat. Sci. Rev.* 149, 248–258.
- Bennike, O., Anderson, N.J., McGowan, S., 2010. Holocene palaeoecology of southwest Greenland inferred from macrofossils in sediments of an oligosaline lake. *J. Paleolimnol.* 43, 787–798.
- Bennike, O., Björck, S., 2002. Chronology of the last deglaciation of Greenland. *J. Quat. Sci.* 17, 211–219.
- Berger, A., Loutre, M.F., 1991. Insolation values for the climate of the last 10 million years. *Quat. Sci. Rev.* 4, 297–317.
- Bjørk, A.A., Kjær, K.H., Korsgaard, N.J., Khan, S.A., Kjeldsen, K.K., Andresen, C.S., Box, J.E., Larsen, N.K., Funder, S., 2012. An aerial view of 80 years of climate-related glacier fluctuations in southeast Greenland. *Nat. Geosci.* <https://doi.org/10.1038/Ngeo1481>.
- Blaauw, M., 2010. Methods and code for 'classical' age-modelling of radiocarbon sequences. *Quat. Geochronol.* 5, 512–518.
- Bolch, T., Sørensen, L.S., Simonsen, S.B., Molg, N., Machguth, H., Rastner, P., Paul, F., 2013. Mass loss of Greenland's glaciers and ice caps 2003–2008 revealed from ICESat laser altimetry data. *Geophys. Res. Lett.* 40, 875–881.
- Bond, G., Kromer, B., Beer, J., Muscheler, R., Evans, M.N., Showers, W., Hoffmann, S., Lotti Bond, R., Hajdas, I., Bonani, G., 2001. Persistent solar influence on North Atlantic climate during the Holocene. *Science* 294, 2130–2136.
- Borchers, B., Marrero, S., Balco, G., Caffee, M., Goehring, B., Lifton, N., Nishiizumi, K., Phillips, F., Schaefer, J., Stone, J., 2016. Geological calibration of spallation production rates in the CRONUS-Earth project. *Quat. Geochronol.* 31, 188–198.
- Briner, J.P., McKay, N.P., Axford, Y., Bennike, O., Bradley, R.S., de Vernal, A., Fisher, D., Francis, P., Fréchette, B., Gajewski, K., Jennings, A., Kaufman, D.S., Miller, G., Rouston, C., Wagner, B., 2016. Holocene climate change in Arctic Canada and Greenland. *Quat. Sci. Rev.* 147, 340–364.
- Bull, C., 1963. Glaciological reconnaissance of the Sukkertoppen ice cap, south-west Greenland. *J. Glaciol.* 4, 813–816.
- Cambridge West Greenland Glaciological Expedition, 1958. General Report. On file at Scott Polar Research Institute, Cambridge. Unpublished.
- Chiverrell, R.C., Thorndycraft, V.R., Hoffmann, T.O., 2011. Cumulative probability functions and their role in evaluating the chronology of geomorphological events during the Holocene. *J. Quat. Sci.* 26, 76–85.
- Citterio, M., Paul, F., Ahlstrom, A.P., Jepsen, H.F., Weidick, A., 2010. Remote sensing of glacier change in West Greenland: accounting for the occurrence of surge-type glaciers. *Ann. Glaciol.* 50, 70–80.
- Clark, P.U., Dyke, A.S., Shakun, J.D., Carlson, A.E., Clark, J., Wohlfarth, B., Mitrovica, J.X., Hostettler, S.W., McCabe, A.M., 2009. The last glacial maximum. *Science* 325, 710–714.
- Clark, P.U., Marshall, S.J., Clarke, G.K.C., Hostettler, S.W., Licciardi, J.M., Teller, J.T., 2001. Freshwater forcing of abrupt climate change during the last glaciation. *Science* 293, 283–287.
- Cronauer, S.L., Briner, J.P., Kelley, S.E., Zimmerman, S.R.H., Morlighem, M., 2016. ^{10}Be dating reveals early-Holocene age of the Drygalski Moraines in central West Greenland. *Quat. Sci. Rev.* 147, 59–68.
- Croudace, I.W., Rindby, A., Rothwell, R.G., 2006. ITRAX: description and evaluation

- of new multi-function X-ray core scanner. In: Rothwell, R.G. (Ed.), New Techniques in Sediment Core Analysis: Special Publications, vol. 267. Geological Society, London, pp. 193–207.
- Dahl, S.O., Bakke, J., Lie, Ø., Nesje, A., 2003. Reconstruction of former glacier equilibrium-line altitudes based on proglacial sites: an evaluation of approaches and selection of sites. *Quat. Sci. Rev.* 22, 275–287.
- de Vernal, A., Hillaire-Marcel, C., Rochon, A., Fréchet, B., Henry, M., Solignac, S., Bonnet, S., 2013. Dinocyst-based reconstructions of sea ice cover concentration during the Holocene in the Arctic Ocean, the northern North Atlantic Ocean and its adjacent seas. *Quat. Sci. Rev.* 79, 111–121.
- Denton, G.H., Karlén, W., 1973. Lichenometry: its application to Holocene moraine studies in southern Alaska and Swedish Lapland. *Arct. Alp. Res.* 5, 347–372.
- Etienne, E., 1940. Expeditionsbericht d'el' Gronland-Expedition der Universität Oxford 1938, vol. 13. Veröffentlichungen des Geophysikalischen Instituts der Universität Leipzig, Zweite Serie, Bd.
- Fleitmann, D., Mudelsee, M., Burns, S.J., Bradley, R.S., Kramers, J., Matter, A., 2008. Evidence for a widespread climatic anomaly at around 9.2 ka before present. *Paleoceanography* 23 (1) (p. n/a-n/a).
- Funder, S., Kjeldsen, K.K., Kjær, K.H., O'Cofaigh, C., 2011. The Greenland ice sheet during the last 300,000 years: a review. *Dev. Quat. Sci.* 15, 699–713.
- Geirsdóttir, Á., Miller, G.H., Larsen, D.J., Olafsdóttir, S., 2013. Abrupt Holocene climate transitions in the northern North Atlantic region recorded by synchronized lacustrine records in Iceland. *Quat. Sci. Rev.* 70, 48–62.
- Gibbons, A.B., Megeath, J.D., Pierce, K.L., 1984. Probability of moraine survival in a succession of glacial advances. *Geology* 12, 327–330.
- Hayward, H.O.'B., 1936. The Oxford University Greenland expedition, 1935. *Geogr. J.* 88, 148–164.
- Henrikssen, N., 2008. Geological History of Greenland Four Billion Years of Earth Evolution. Geological Survey of Denmark and Greenland (GEUS), Copenhagen, pp. 1–272.
- Henry, T.A., 1959. Greenland's Icy Mountains, vol. 2. Visa, Cambridge, pp. 13–15.
- Hippe, K., 2017. Constraining processes of landscape change with combined cosmogenic ^{14}C ^{10}Be analysis. *Quat. Sci. Rev.* 173, 1–19.
- Hippe, K., Lifton, N.A., 2014. Calculating isotope ratios and nuclide concentrations for *in situ* cosmogenic ^{14}C analyses. *Radiocarbon* 56, 1167–1174.
- Holland, M.F.W., 1961. Glaciological observations around mount atter, west Greenland. *J. Glaciol.* 3, 804–812.
- Ingólfsson, O., Frich, P., Funder, S., Humlum, O., 1990. Paleo-climatic implications of an early Holocene glacier advance on Disko-Island, west Greenland. *Boreas* 19, 297–311.
- Jiang, H., Muscheler, R., Björck, S., Seidenkrantz, M.S., Olsen, J., Sha, L., Sjolte, J., Eiríksson, J., Ran, L., Knudsen, K.-L., Knudsen, M.F., 2015. Solar forcing of Holocene summer sea-surface temperatures in the northern North Atlantic. *Geology* 43, 203–206.
- Jennings, A., Andrews, J., Pearce, C., Wilson, L., Ólafsdóttir, S., 2015. Detrital carbonate peaks on the Labrador shelf, a 13–7 ka template for freshwater forcing from the Hudson Strait outlet of the Laurentide Ice Sheet into the subpolar gyre. *Quat. Sci. Rev.* 107, 62–80.
- Jomelli, V., et al., 2016. Paradoxical cold conditions during the medieval climate anomaly in the western Arctic. *Sci. Rep.* 6 <https://doi.org/10.1038/srep32984>.
- Jongma, J.I., Prange, M., Renssen, H., Schulz, M., 2007. Amplification of Holocene multicentennial climate forcing by mode transitions in North Atlantic overturning circulation. *Geophys. Res. Lett.* 34. <https://doi.org/10.1029/2007GL030642>.
- Kaplan, M.R., Wolfe, A.P., Miller, G.H., 2002. Holocene environmental variability in southern Greenland inferred from lake sediments. *Quat. Res.* 58, 149–159.
- Kelly, M., 1980. The status of the Neoglacial in western Greenland. *Rapport Greenland Geol. Survey* 96, 1–24.
- Kelly, M., 1985. A review of the Quaternary geology of western Greenland. In: Andrews, J.T. (Ed.), Quaternary Environments in Eastern Canadian Arctic, Baffin Bay and Western Greenland. Allen and Unwin, Boston, pp. 461–501.
- Kelly, M.A., Lowell, T.V., 2009. Fluctuations of local glaciers in Greenland during latest Pleistocene and Holocene time. *Quat. Sci. Rev.* 28, 2088–2106.
- Kelley, S.E., Briner, J.P., Young, N.E., 2013. Rapid ice retreat in Disko Bugt supported by ^{10}Be dating of the last recession of the western Greenland Ice Sheet. *Quat. Sci. Rev.* 82, 13–22.
- Kelley, S.E., Briner, J.P., Zimmerman, S.R., 2015. The influence of ice marginal setting on early Holocene retreat rates in central West Greenland. *J. Quat. Sci.* 30, 271–280.
- Kobashi, T., Kawamura, K., Severinghaas, J.P., Barnola, J.M., Nakagawa, T., Vinther, B.M., Johnsen, S.J., Box, J.E., 2011. High variability of Greenland surface temperature over the past 4000 years estimated from trapped air in an ice core. *Geophys. Res. Lett.* 38. <https://doi.org/10.1029/2011GL049444>.
- Kobashi, T., Box, J.E., Vinther, B.M., Goto-Azuma, K., Blunier, T., White, J.W.C., Nakagawa, T., Andresen, C.S., 2015. Modern solar maximum forced late twentieth century Greenland cooling. *Geophys. Res. Lett.* 42 <https://doi.org/10.1002/2015GL064764>.
- Kobashi, T., et al., 2017. Volcanic influence on centennial to millennial Holocene Greenland temperature change. *Sci. Rep.* 7 <https://doi.org/10.1038/s41598-017-01451-7>.
- La Farge, C., Williams, K.H., England, J.H., 2013. Regeneration of Little Ice Age bryophytes emerging from a polar glacier with implications of totipotency in extreme environments. *Proc. Natl. Acad. Sci. U.S.A.* 110, 9839–9844.
- Larsen, D.J., Miller, G.H., Geirsdóttir, Á., Thordarson, T., 2011. A 3000-year varved record of glacier activity and climate change from the proglacial lake Hvítárvatn, Iceland. *Quat. Sci. Rev.* 30, 2715–2731.
- Larsen, D.J., Miller, G.H., Geirsdóttir, Á., Ólafsdóttir, S., 2012. Non-linear Holocene climate evolution in the North Atlantic: a high-resolution, multi-proxy record of glacier activity and environmental change from Hvítárvatn, central Iceland. *Quat. Sci. Rev.* 39, 14–25.
- Larsen, N.K., Funder, S., Kjær, K.H., Kjeldsen, K.K., Knudsen, M.F., Linge, H., 2014. Rapid early Holocene ice retreat in West Greenland. *Quat. Sci. Rev.* 92, 310–323.
- Larsen, N.K., Strunk, A., Levy, L.B., Olsen, J., Bjørk, A., Lauridsen, T.L., Jeppesen, E., Davidson, T.A., 2017. Strong altitudinal control on the response of local glaciers to Holocene climate change in southwest Greenland. *Quat. Sci. Rev.* 168, 69–78.
- Lesnek, A.J., Briner, J.P., 2018. Response of a land-terminating sector of the western Greenland Ice Sheet to early Holocene climate change: evidence from ^{10}Be dating in the Søndre Isortoq region. *Quat. Sci. Rev.* 180, 145–156.
- Levy, L.B., Kelly, M.A., Lowell, T., Hall, B., Hempel, L.A., Honsaker, W., Lusas, A.R., Howley, J.A., Axford, Y., 2014. Holocene fluctuations of Brengie ice cap, Scoresby Sund, east Greenland: a proxy for climate along the Greenland Ice Sheet margin. *Quat. Sci. Rev.* 92, 357–368.
- Lifton, N., Goehring, B., Wilson, J., Kubley, T., Caffee, M., 2015. Progress in automated extraction and purification of *in situ* ^{14}C from quartz: results from the Purdue *in situ* ^{14}C laboratory. *Nucl. Instrum. Methods Phys. Res. Sect. B Beam Interact. Mater. Atoms* 361, 381–386.
- Lifton, N., Sate, T., Dunai, T.J., 2014. Scaling *in situ* cosmogenic nuclide production rates using analytical approximations to atmospheric cosmic-ray fluxes. *Earth Planet. Sci. Lett.* 386, 149–160.
- Loewe, F., Bull, C., McCormick, J., Treves, S.B., 1962. Reconnaissance of Sukkertoppen Ice Cap and Adjacent Tasersiaq Area, Southwest Greenland. Report No. 4. Quartermaster Research and Engineering Command, U.S. Army, pp. 1–36.
- Lowell, T.V., Hall, B.L., Kelly, M.A., Bennike, O., Lusas, A.R., Honsaker, W., Smith, C.A., Levy, L.B., Travis, S., Denton, G.H., 2013. Late Holocene expansion of Istvortet ice cap, Liverpool land, east Greenland. *Quat. Sci. Rev.* 63, 128–140.
- Lupker, M., Hippe, K., Wacker, L., Kober, F., Maden, C., Braucher, R., Bourles, D., Romani, J.R.V., Wieler, R., 2015. Depth-dependence of the production rate of *in situ* C-14 in quartz from the Leymon High core, Spain. *Quat. Geochronol.* 28, 80–87.
- Machguth, H., Thomsen, H.H., Weidick, A., Ahlstrom, A.P., Abermann, J., Andersen, M.L., Andersen, S.B., Bjørk, A.A., Box, J.E., Braithwaite, R.J., Boggild, C.E., Citterio, M., Clement, P., Colgan, W., Fausto, R.S., Gleie, K., Gubler, S., Hasholt, B., Hynek, B., Knudsen, N.T., Larsen, S.H., Mernild, S.H., Oerlemans, J., Oerter, H., Olesen, O.B., Smeets, C.J.P.P., Steffen, K., Stober, M., Sugiyama, S., van As, D., van den Broeke, M.R., van de Wal, R.S.W., 2016. Greenland surface mass-balance observations from the ice-sheet ablation area and local glaciers. *J. Glaciol.* 62, 861–887.
- Marcott, S.A., Shakun, J.D., Clark, P.U., Mix, A.C., 2013. A reconstruction of regional and global temperature for the past 11,300 years. *Science* 339, 1198–1201.
- Margreth, A., Dyke, A.S., Gosse, J.C., Telka, A.M., 2014. Neoglacial ice expansion and late Holocene cold-based ice cap dynamics on Cumberland Peninsula, Baffin Island, Arctic Canada. *Quat. Sci. Rev.* 91, 242–256.
- Mayewski, P.A., Rohling, E.E., Stager, J.C., Karlén, W., Maasch, K.A., Meeker, L.D., Meyerson, E.A., Gasse, F., van Kreveld, S., Holmgren, K., Lee-Thorp, J., Rosqvist, G., Rack, F., Staubwasser, M., Schneider, R.R., Steig, E.J., 2004. Holocene climate variability. *Quat. Res.* 62, 243–255.
- McManus, J.F., Francois, R., Gherardi, J.M., Keigwin, L.D., Brown-Leger, S., 2004. Collapse and rapid resumption of Atlantic meridional circulation linked to deglacial changes. *Nature* 428, 834–837.
- Miller, G.H., Briner, J.P., Lifton, N.A., Finkel, R.C., 2006. Limited ice-sheet erosion and complex exposure histories derived from *in situ* cosmogenic ^{10}Be , ^{26}Al , and ^{14}C on Baffin Island, Arctic Canada. *Quat. Geochronol.* 1, 74–85.
- Miller, G.H., Briner, J.P., Refsnider, K.A., Lehman, S.J., Geirsdóttir, Á., Larsen, D.J., Southon, J.R., 2013b. Substantial agreement on the timing and magnitude of Late Holocene ice cap expansion between East Greenland and the eastern Canadian Arctic: a commentary on Lowell et al., 2013b. *Quat. Sci. Rev.* 77, 239–245.
- Miller, G.H., Geirsdóttir, Á., Zhong, Y., Larsen, D.J., Otto-Bliesner, B.L., Holland, M.M., Bailey, D.A., Refsnider, K.A., Lehman, S.J., Southon, J.R., Anderson, C., Björnsson, H., Thordarson, T., 2012. Abrupt onset of the Little Ice Age triggered by volcanism and sustained by sea-ice/ocean feedbacks. *Geophys. Res. Lett.* 39, L02708.
- Miller, G.H., Landvik, J.Y., Lehman, S.J., Southon, J.R., 2017. Episodic Neoglacial snowline descent and glacier expansion on Svalbard reconstructed from the C-14 ages of ice-entombed plants. *Quat. Sci. Rev.* 155, 67–78.
- Miller, G.H., Lehman, S.J., Refsnider, K.A., Southon, J.R., Zhong, Y.F., 2013a. Unprecedented recent summer warmth in Arctic Canada. *Geophys. Res. Lett.* 40, 5745–5751.
- Moffa-Sánchez, P., Born, A., Hall, I.R., Thornalley, D.J.R., Barker, S., 2014. Solar forcing of North Atlantic surface temperature and salinity over the past millennium. *Nature* 527, 275–278.
- Mott, P.G., 1937. The Oxford university Greenland expedition, west Greenland, 1936. *Geogr. J.* 90, 315–334.
- Nesje, A., 1992. A Piston Corer for Lacustrine and marine Sediments: Arctic and Alpine Research, pp. 257–259.
- Nishiizumi, K., Imamura, M., Caffee, M.W., Southon, J.R., Finkel, R.C., McAninch, J., 2007. Absolute calibration of ^{10}Be AMS standards. *Nucl. Instrum. Methods Phys. Res. Sect. B Beam Interact. Mater. Atoms* 258, 403–413.
- O'Hara, S.L., Briner, J.P., Kelley, S.E., 2017. A ^{10}Be chronology of early Holocene local glacier moraines in central West Greenland. *Boreas* 46, 655–666.

- Oerlemans, J., 2005. Extracting a climate signal from 169 glacier records. *Science* 308, 675–677.
- Paillet, D., Labeyrie, L.D., Yiou, P., 1996. AnalySeries 1.0: a Macintosh software for the analysis of geophysical time-series. *Eos* 77, 379.
- Phillips, F.M., Argento, D.C., Balco, G., Caffee, M.W., Clem, J., Dunai, T.J., Finkel, R., Goehring, B., Gosse, J.C., Hudson, A.M., Jull, A.T., 2016. The CRONUS-Earth project: a synthesis. *Quat. Geochronol.* 31, 119–154.
- Rasmussen, S.O., Vinther, B.M., Clausen, H.B., Andersen, K.K., 2007. Early Holocene climate oscillations recorded in three Greenland ice cores. *Quat. Sci. Rev.* 26 (15–16), 1907–1914.
- Rastner, P., Bolch, T., Molg, N., Machguth, H., Le Bris, R., Paul, F., 2012. The first complete inventory of the local glaciers and ice caps on Greenland. *Cryosphere* 6, 1483–1495.
- Reimer, P.J., Bard, E., Bayliss, J.W., Beck, P.G., Blackwell, C., Bronk Ramsey, C.E., Buck, H., Cheng, R.L., Edwards, M., Friedrich, P.M., Grootes, T.P., Guilderson, H., Haflidason, I., Hajdas, C., Hatte, T.J., Heaton, D.L., Hoffmann, A.G., Hogg, K.A., Hughen, K.F., Kaiser, B., Kromer, S.W., Manning, M., Niu, R.W., Reimer, D.A., Richards, E.M., Scott, J.R., Southon, R.A., Staff, C., Turney, S.M., van der Plicht, J., 2013. IntCal13 and Marine13 radiocarbon age calibration curves -50,000 Years cal BP. *Radiocarbon* 55, 1869–1887.
- Roberts, D.H., Long, A.J., Davies, B.J., Simpson, M.J., Schnabel, C., 2010. Ice stream influence on west Greenland ice sheet dynamics during the last glacial maximum. *J. Quat. Sci.* 25, 850–864.
- Roberts, D.H., Long, A.J., Schnabel, C., Davies, B.J., Xu, S., Simpson, M.J.R., Huybrechts, P., 2009. Ice sheet extent and early deglacial history of the southwestern sector of the Greenland Ice Sheet. *Quat. Sci. Rev.* 28, 2760–2773.
- Røthe, T.O., Bakke, J., Vasskog, K., Gjerde, M., D'Andrea, W.J., Bradley, R.S., 2015. Arctic Holocene glacier fluctuations reconstructed from lake sediments at Mitrahavvøya, Spitsbergen. *Quat. Sci. Rev.* 109, 111–125.
- Rothwell, R.G., Hoogakker, B., Thomson, J., Croudace, I.W., Frenz, M., 2006. Turbidite emplacement on the southern Balearic Abyssal Plain (western Mediterranean Sea) during Marine Isotope Stages 1–3: an application of ITRAX XRF scanning of sediment cores to lithostratigraphic analysis. In: Rothwell, R.G. (Ed.), *New Techniques in Sediment Core Analysis*. Geological Society, London, pp. 65–78. Special Publications, 267.
- Schneider, D.P., Ammann, C.M., Otto-Bliesner, B.L., Kaufman, D.S., 2009. Climate response to large, high-latitude and low-latitude volcanic eruptions in the Community Climate System Model. *J. Geophys. Res.* 114, D15101.
- Schweinsberg, A.D., Briner, J.P., Miller, G.H., Bennike, O., Thomas, E.K., 2017. Local glaciation in West Greenland linked to North Atlantic ocean circulation during the Holocene. *Geology* 45, 195–198.
- Sigl, M., et al., 2015. Timing and climate forcing of volcanic eruptions for the past 2,500 years. *Nature* 523, 543–549.
- Smith, J.G., 2003. Aspects of the loss-on-ignition (LOI) technique in the context of clay-rich, glaciolacustrine sediments. *Geogr. Ann. Phys. Geogr.* 85, 91–97.
- Solomina, O.N., et al., 2015. Holocene glacier fluctuations. *Quat. Sci. Rev.* 111, 9–34.
- Strunk, A., Knudsen, M.F., Egholm, D.L., Jansen, J.D., Levy, L.B., Jacobsen, B.H., Larsen, N.K., 2017. One million years of glaciation and denudation history in west Greenland. *Nat. Commun.* 8, 14199.
- Stuiver, M., Reimer, P.J., Reimer, R., 2005. CALIB radiocarbon Calibration. Execute version, 5.
- Sugden, D.E., 1972. Deglaciation and isostasy in the Sukkertoppen ice cap area, west Greenland. *Arct. Alp. Res.* 4, 97–117.
- Sugden, D.E., Mott, P.G., 1940. Oxford university Greenland expedition, 1938. *Geogr. J.* 95, 43–51.
- Ten Brink, N.W., 1975. Holocene history of the Greenland ice sheet based on radiocarbon dated moraines in West Greenland. *Meddelelser om Grønland* 44 (113).
- Thomas, E.K., Szymanski, J., Briner, J.P., 2010. Holocene alpine glaciation inferred from lacustrine sediments on northeastern Baffin Island, Arctic Canada. *J. Quat. Sci.* 25, 146–161.
- Tomkins, J.D., Antoniades, D., Lamoureux, S.F., Vincent, W.F., 2008. A simple and effective method for preserving the sediment–water interface of sediment cores during transport. *J. Paleolimnol.* 40, 577–582.
- Trouet, V., Esper, J., Graham, N.E., Baker, A., Scourse, J.D., Frank, D.C., 2009. Persistent positive North Atlantic oscillation mode dominated the medieval climate anomaly. *Science* 3, 78–80.
- Vasskog, K., Langebroek, P.M., Andrews, J.T., Nilsen, J.E.Ø., Nesje, A., 2015. The Greenland Ice Sheet during the last glacial cycle: current ice loss and contribution to sea level rise from a palaeoclimatic perspective. *Earth Sci. Rev.* 150, 45–67.
- Vasskog, K., Paasche, Ø., Nesje, A., Boyle, J.F., Birks, H.J.B., 2012. A new approach for reconstructing glacier variability based on lake sediments recording input from more than one glacier. *Quat. Res.* 77, 192–204.
- Vinther, B.M., Clausen, H.B., Johnsen, S.J., Rasmussen, S.O., Andersen, K.K., Buchardt, S.L., Dahl-Jensen, D., Seierstad, I.K., Siggaard-Andersen, M.L., Seffensen, J.P., Svensson, A., Olsen, J., Heinemeier, J., 2006. A synchronized dating of three Greenland ice cores throughout the Holocene. *J. Geophys. Res.* 111. <https://doi.org/10.1029/2005JD006921>.
- Wanner, H., Beer, J., Bütkofer, J., Crowley, T.J., Cubasch, U., Flückiger, J., Goosse, H., Grosjean, M., Joos, F., Kaplan, J.O., 2008. Mid-to-Late Holocene climate change: an overview. *Quat. Sci. Rev.* 27, 1791–1828.
- Wanner, H., Solomina, O., Grosjean, M., Ritz, S.P., Jetel, M., 2011. Structure and origin of Holocene cold events. *Quat. Sci. Rev.* 30, 3109–3123.
- Weidick, A., Bøggild, C.E., Knudsen, N.T., 1992. Glacier inventory and Atlas of west Greenland. *Grønlands Geologiske Undersøgelse Rapport* 158, 1–194.
- Weidick, A., 1968. Observations on some Holocene glacier fluctuations in West Greenland. *Meddelelser om Grønland* 165, 1–202.
- Weidick, A., Bennike, O., 2007. Quaternary glaciation history and glaciology of Jakobshavn Isbrae and the Disko Bugt region, west Greenland: a review. *Geol. Surv. Den. Greenl. Bull.* 14, 1–78.
- Wiles, G.C., D'Arrigo, R.D., Villalba, R., Calkin, P.E., Barclay, D.J., 2004. Century-scale solar variability and Alaskan temperature change over the past millennium. *Geophys. Res. Lett.* 31. <https://doi.org/10.1029/2004GL020050>.
- Williams, A.N., 2012. The use of summed radiocarbon probability distributions in archaeology: a review of methods. *J. Archaeol. Sci.* 39, 578–589.
- Winsor, K., Carlson, A.E., Caffee, M.W., Rood, D.H., 2015a. Rapid last-deglacial thinning and retreat of the marine-terminating southwestern Greenland ice sheet. *Earth Planet Sci. Lett.* 426, 1–12.
- Winsor, K., Carlson, A.E., Welke, B., Reilly, B., 2015b. Early deglacial onset of southwestern Greenland ice-sheet retreat on the continental shelf. *Quat. Sci. Rev.* 128, 117–126.
- Young, N.E., Briner, J.P., Stewart, H.A.M., Axford, Y., Csatho, B., Rood, D.H., Finkel, R.C., 2011. Response of Jakobshavn Isbrae, Greenland, to Holocene climate change. *Geology* 39, 131–134.
- Young, N.E., Schaefer, J.M., Briner, J.P., Goehring, B.M., 2013a. A ^{10}Be production rate calibration for the Arctic. *J. Quat. Sci.* 28, 515–526.
- Young, N.E., Briner, J.P., Rood, D.H., Finkel, R.C., Corbett, L.B., Bierman, P.R., 2013b. Age of the Fjord Stade moraines in the Disko Bugt region, western Greenland, and the 9.3 and 8.2 ka cooling events. *Quat. Sci. Rev.* 60, 76–90.
- Young, N.E., Schweinsberg, A.D., Briner, J.P., Schaefer, J.M., 2015. Glacier maxima in Baffin Bay during the medieval warm period coeval with Norse settlement. *Science Advances* 1, e1500806.
- Yu, S., Colman, S.M., Lowell, T.V., Milne, G.A., Fisher, T.G., Breckenridge, A., Boyd, M., Teller, J.T., 2010. *Science* 4, 1262–1266.
- Zhong, Y., Miller, G.H., Otto-Bliesner, B.L., Holland, M.M., Bailey, D.A., Schneider, D.P., Geirsdóttir, Á., 2011. Centennial-scale climate change from decadally-paced explosive volcanism: a coupled sea ice-ocean mechanism. *Clim. Dynam.* 37, 2373–2387.